April 2015

Development of a Stand-alone Microfluidic Device

Fayez Abdullah Alfayez
Worcester Polytechnic Institute

Joseph Michael Brown
Worcester Polytechnic Institute

Mercedes Destine Brown
Worcester Polytechnic Institute

Development of a Stand-alone Microfluidic Device

With Fiber Optical Sensor, Self-Powered Pump, and Cellphone Based Imaging Platform

Fayez Alfayez, Joseph Brown, and Mercedes Brown
Advisors: Prof. Yuxiang Liu and Prof. Zhikun Hou, ** yliu11@wpi.edu
Dept. of Mechanical Engineering, Worcester Polytechnic Institute, Worcester, MA

Abstract

Microfluidics, also referred to as lab-on-a-chip (LOC), is an emerging technology in which fluids can be precisely manipulated using micro-scale devices. LOC has found various applications in healthcare, on-chip chemical analysis, and inkjet printing. In this work, we designed a stand-alone LOC system that includes a self-powered pump, an optical fiber-based flow detection sensor, and smartphone-based imaging platform. The designed device aims to combine multiple physical concepts into one, integrated, self-sufficient, and modular chip-based system. Fluidic samples can be pumped into the device by a single finger push, without a need of external pump or electrical power supply, and particles with the size of a few tens of micrometers (similar size of single red blood cells) can be imaged without using any microscope. To the best of our knowledge, this is the first time all necessary functions of lab-on-a-chip devices, including pumping, characterization, and imaging, are integrated on a single chip in which the only needed external device is a smartphone to work properly. Various fabrication techniques were developed and evaluated. The designed devices are fabricated and characterized to prove the concept. The team developed both fundamental understandings and hands-on experience on microfluidic systems, while the designs show great potential for a fully integrated device. Future work can utilize the methods developed in this work to fabricate and test alternate designs for a working and commercially producible LOC device.

1. Introduction

Microfluidics, also referred to as miniaturized total analysis systems (mTASs) or Lab-on-a-Chip (LoC), is the technology where fluids can be precisely manipulated using micro-scale devices. [1] The field of microfluidics is characterized by the study and manipulation of fluids at the sub-millimeter length scale, and the device is generally a single chip of only millimeters to a few centimeters in size [2], as shown in Figure 1.

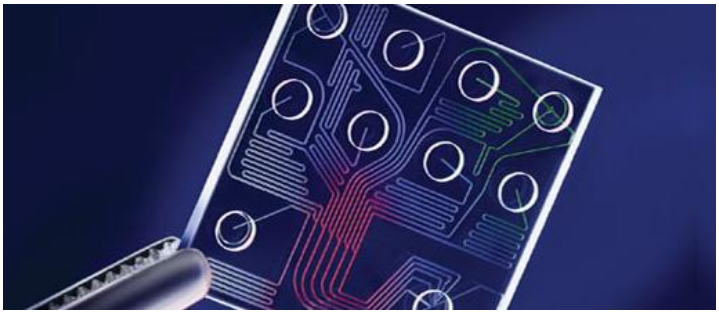

Figure 1 Example of a Lab-on-a-Chip, from Amplitude Systems [3]

1.1 Lab-on-a-Chip Motivation

LoC technology is a growing field with significant potential in the healthcare, chemical and material industries. With this technology, various laboratory functions and analyses that typically require bulky and sophisticated testing equipment can be performed on a single chip only millimeters or micrometers in size. In order to make these devices commercially available, they must be more self-sustaining and user friendly than they currently are. There is also a need to improve and expedite the fabrication of such devices for laboratories that have limited access to full fabrication resources. This project developed easier fabrication methods for a lab-on-a-chip device that is self-powered and utilizes fiber optic and cell phone technology to make lab-on-a-chip even more robust and user friendly.

Lab-on-a-chip technology has significant applications in chemistry and biomedicine, since it allows the user to examine fluidic samples at a microscopic level, [2]. As such, with lab-on-a-chip one can analyze specimens as small as an individual cell or a strand of DNA. There are limitless possibilities of how lab-on-a-chip can be applied. Yehaya H. Ghallab and Wael Badawy [2] assert that someday, common consumers could use lab-on-chip systems to test for pregnancy, HIV, and some types of cancer, [2]. A thorough chemical analysis could be at the fingertips of scientists and civilians alike.

The small size of the chips allows them to measure large amounts of data for a small sample volume. [2] It also means that they have the potential to be very portable, with not much instrumentation required to collect data. LOC devices are fairly easy to prototype at a low cost and are easily disposable. [2] However, improvements to their fabrication, data collection and pumping abilities will make this technology more accessible to common users.

1.2 Background

A typical microfluidic device includes driving action, laboratory function, and data collection. A mechanical pump that pushes the fluid through the channels can provide the driving action of an LOC. Some laboratory procedure, such as particle separation of flow observation, is then performed on the fluid of study. Finally, some type of data must be output in order to make LOC analysis meaningful.

1.2.1 Pumping

Flow rate control is important to the operation of a Lab-on-a-Chip, as some tests can only be performed with a particular flow rate. [4] There are numerous methods of controlling flow rate. In a laboratory setting, a mechanical pump such as the LongerPump LSP02-1B Dual Channels Syringe Pump can easily be used to set a flow rate for controlled testing. However, it is not feasible to use this large piece of equipment for integrated Lab-on-a-Chip use.

Physical injection refers to a syringe full of liquid that is physically being operated by a human being. The liquid is being pumped by hand using a syringe into the system. It is very difficult maintain a steady, constant flow in the system; also extra lab equipment is needed for the mechanical method, which is the opposite of our goals.

One approach to fluid manipulation is a method called electrowetting [5]. This concept utilizes an electric field to modify the wetting properties of the sample. This not only allows the user to control the speed of the flow, but also the direction.

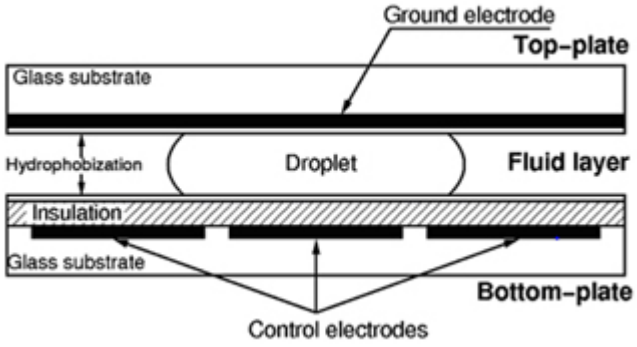

Figure 2 Integration of an electric field on the bottom plate, Royal et al, *IEE Sensors Journal*, 2013 [5]

This method also does not need fixed channels. It would be possible to manipulate the flow into any direction, speed, and path on top of the electrodes.

While this design was interesting and allowed more interaction and manipulation with the flow, there was still the fact that it relied on electricity. The device would need to retain a charge in order to activate and work.

Another concept that was greatly considered was the self-powered pump. This pump required no equipment, no electricity, and could be activated by the simple press of a finger. Integrating this design would make our LOC even more stand-alone.

A self-powered pump such as the one described in *Self-powered Imbibing Microfluidic Pump by Liquid Encapsulation* [6] requires no outside power or complicated machine work. Rather than relying on electricity, this pump primarily utilizes capillary systems as well as fluidic forces. The design is rather simple and primarily relies on the following two equations:

$$\left(\frac{r}{r_0}\right)^2\left(ln\frac{r}{r_0}-\frac{1}{2}\right)+\frac{1}{2}=\frac{\gamma a cos\theta_w}{6\mu r_0^2}t \qquad (1)$$

$$Q=\frac{dV}{dt}=\frac{\theta_c}{360°}\phi 2\pi rh\frac{dr}{dt} \qquad (2)$$

where r is the radius of the wetted area and theta is the area of the fan area. These parameters are main areas of focus. g (gamma) is the surface tension and μ the viscosity.

As Figure 3 shows, the device comprises of a large circular area that is connected by channels to a fan in which a porous material absorbs flowing liquid. The size of the channels and angle of the fan can be dimensioned to meet the geometric and operational needs of the device. Once the chip has been prefilled, the pump can begin its functions. The next step is placing the sample solution on its proper channel inlet; the chip should also have all opening closed. When the solution is in place, all that is needed to activate the pump is the simple press of a finger. This force pushes the liquid, where it will make contact with the porous material in the fan. However, the pump will only continue to work when there is liquid present; once the pre-filled liquid runs out, the pump will cease to work.

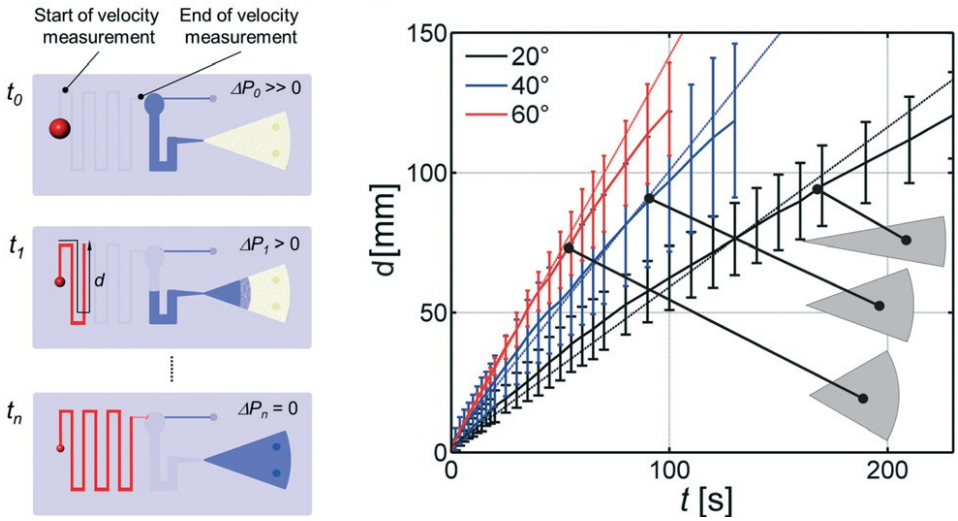

Figure 3 Demonstration of how the angle of the fan affects the flow rate, Kokai et al, *Self-powered Imbibing Microfluidic Pump, 2014* [6]

1.2.2 Sample Manipulation/Laboratory Function

Once the fluidic sample is being pumped through the device, it can be manipulated to serve some laboratory function. One such method of sample manipulation is separation of particles based on their size. [7] Once separated, the different sized particles could be analyzed separately based on their optical features.

The technique is simple, inexpensive, and high-throughput. It cleverly manipulates the channel's geometry to control the net forces acting on the moving particles, which allows us to predict their trajectory. Moreover, researchers found that spiral shaped channels can have high separation efficiency. [8]

1.2.2.1 Particles in a straight channel

In order to understand the physics of the inertial focusing and separation method, one need to acknowledge the inertial and viscous effect of the moving fluid in the system [7 - 11]. Reynolds can give a numeric indicator of this relation. Moreover, the fluid behavior can be model by solving the Navier-Stokes Equation:

$$\rho\left(\frac{\partial u}{\partial t} + u \cdot \nabla \mathrm{u}\right) = -\nabla \mathrm{p} \nabla^2 u + f \qquad (3)$$

where ρ is density, u the fluid velocity, t is time, and f is the vector force field of a body acting on the fluid. The dominant forces that act on circular buoyant moving body are the Secondary-Flow Drag Force and inertial lift, which is composed of wall interaction force and the shear gradient lift force.

1.2.2.2 Wall interaction force

A particle flowing through a channel will interact with the wall, and this interaction results in force that is directed away from the wall. This interaction has two effects: first, particles near the wall will have slow velocity relative to the average flow velocity of the fluid. Second, pressure gradient across the particle will cause the particle to move to the relatively faster velocity side. Wall interaction force depends strongly on the Reynolds number and the particle position and size. In rectangular channels, this will cause the particles to move to the center of the channel, as shown in Figure 4a. The wall force can be mathematically described as:

$$F_{WI} = C_{WI} \rho {U_{\max}}^2 \frac{a^6}{{D_h}^4} \qquad (4)$$

where C_{wi} is the lift coefficient dependent upon Reynolds numbers and particle positions, ρ is the average fluid density, U_{max} is the maximum fluid velocity in the channel, a is the particle diameter, and D_h is the hydraulic diameter. [14]

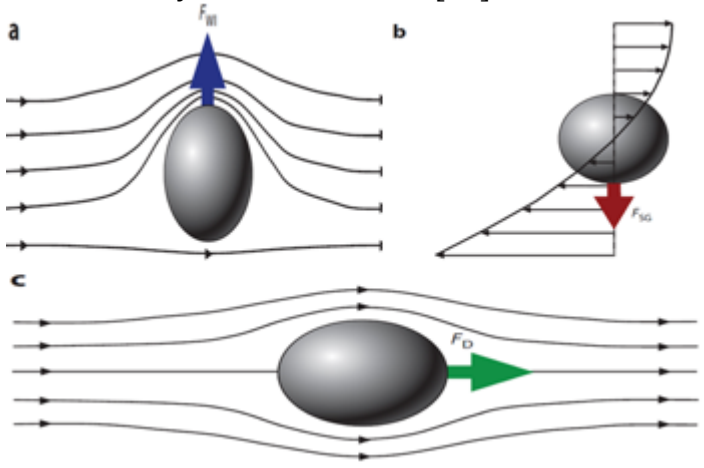

Figure 4 Forces acting on moving particles, Martel et al, *Inertial Focusing in Microfluidics*, 2014, [9]

1.2.2.3 Shear gradient lift force

A typical velocity profile in a microfluidic channel is laminar and thus shear stress

differs across the particle sides. A particle that experiences different velocities on its sides (relative velocities) will experience force exerted by the fluid flowing around the particle to compensate for this difference. In a rectangular channel this force is directed toward the walls of the channels, and the shear gradient force is zero at the center of the channel. This shear gradient force depends largely on the Reynolds number and the particle position and size (see Figure 3 b). The shear gradient lift force can be mathematically described as:

$$F_{WI} = C_{SG}\rho U_{\max}{}^2 \frac{a^3}{D_h} \qquad (5)$$

where C_{sg} is a lift coefficient dependent upon the Reynolds numbers and the position of the particles, r is the average fluid density, U_{max} is the maximum fluid velocity in the channel, a is the particle diameter, and D_h is the hydraulic diameter.

1.2.2.4 Particles in a curved channel

Furthermore, researchers found that the Dean drag force can be manipulated to control the position of the moving particles. This secondary effect, which is known as the Dean flow, creates velocity field perpendicular to the moving fluid direction. The velocity field creates a drag force that that moves the particles, (see Figure 4 Forces acting on moving particles c). The secondary Dean flow can be created at high Reynolds Number or in a curved channel.

The Dean number serves as a numerical indicator of how strong this effect is and can be calculated using the following equation:

$$D = Re(\frac{d}{2R})^{0.5} \qquad (6)$$

where Re is the Reynolds number, d is the diameter, and R is the radius of curvature.

When fluid moves in a curved channel, the mismatch of the outer wall and the inner wall velocities create pressure gradient. This pressure difference generates recirculation of the fluid in the perpendicular direction of the moving fluid, as shown in Figure 5. Moreover, the design of the channels can restrict what position the particle should occupy, as Figure 5 displays. When the velocity of the Dean flow is known, the resulting force can be simply predicted using drag force equation, which is described as:

$$F_D = 6\pi\mu a U_{SF} \qquad (7)$$

where μ is the dynamic viscosity, a is the particle diameter, and U_{sf} is the speed of the fluid relative to the particle.

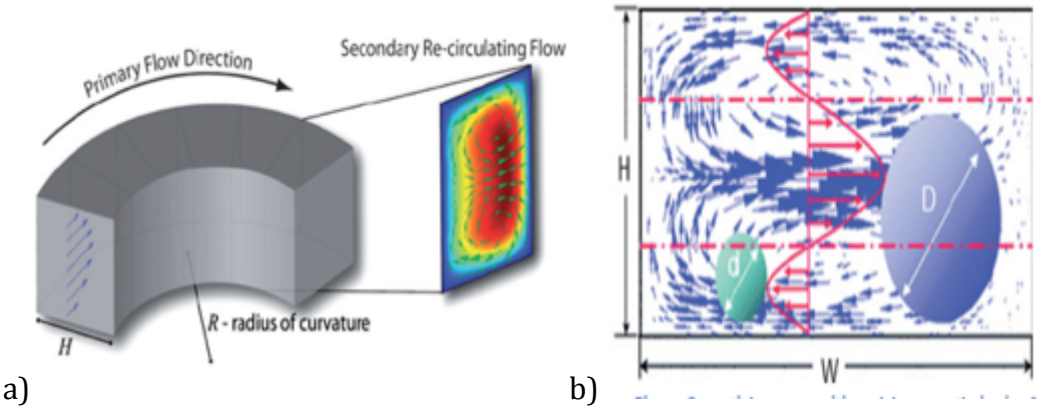

Figure 5 a) Dean Flow (recirculation flow) b) Particles are positioned based on their size for a chosen height and width of the channels [8]

Researchers have innovated double spiral microfluidic channels that are capable of separating tumor cells with 88.5% tumor recovery [7]. The interaction of the inertial lift force and the secondary dean flow force can be used to manipulate the fluid inside the curved channel. In order to optimize the separating system, an experimental testing of channels with different sizes will be fabricated and tested.

1.2.3 Physics of an Evanescent Field

In an optical fiber, light propagates in the fiber core by the principle of Total Internal Reflection (TIR), which can be understood by Snell's law, and the reflection law:

$$n_1 sin\theta_1 = n_2 sin\theta_2 \quad \text{Snell's law (8)}$$
$$\theta_1 Incident = \theta_1 Reflected \quad \text{Reflection law (9)}$$

where:
n_1 is the refractive index of the medium the light is leaving
θ_1 is the incident angle between the light beam and the normal, and the angle between the normal and the reflected beam.
$n_2$is the refractive index of the medium the light is entering
θ_2 is the refractive angle between the light ray and the normal

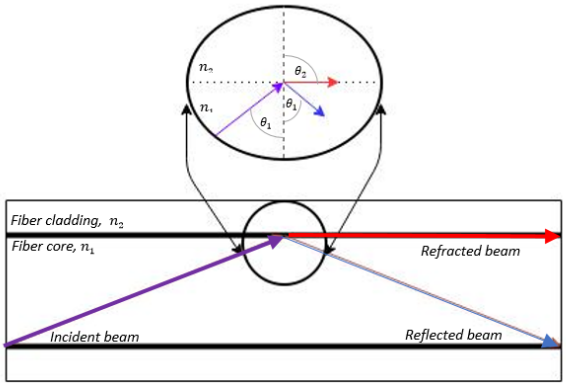

Figure 6 A ray of light inside an optical fiber. The purple arrow is the incident ray, red arrow is the refracted beam, and blue arrow is the reflected beam. All directions follow Snell's law and the reflection law.

In order to confine most of the light energy in a multimode fiber, the refractive angle (θ_2) between the purple arrow and the red arrow in Figure 6 must be 90 degree. In doing so, most of the energy that is given by the purple arrow in Figure 6 will be confined inside the fiber. By substituting 90 degree for the refractive angle (θ_2) in Snell's, law one can obtain the minimum incident angle, or critical angle. A light beam that is incident at larger angle than the minimum incident angle will go under TIR, where most of the energy is confined in the fiber core. However, a light beam that is incident at smaller angle than the minimum incident angle will experience significant power loss. Using Snell's law and substituting 90 degrees for θ_2, 1.45 for n_1(the core refractive index), one can plot the minimum incident angle as a function of n_2, as shown in

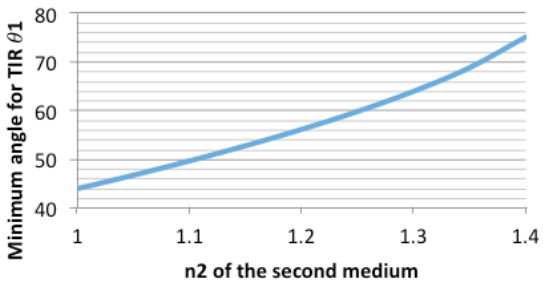

Figure 7 Graphical representation of Snell's law, where θ_2 = 90 degree and n1 is 1.45

As Figure 7 shows, the refractive index of the secondary medium is relatively small compared to that of the fiber core. For example, when $n_{cladding}$= 1.1, one can expect high optical power transmission to be measured at the end of the fiber since light rays inside the fiber have large ranges of angles to be guided down the fiber. However, when the refractive index of the secondary medium is respectively large, for example $n_{cladding}$=1.3, low optical power will be measured at the fiber end. Therefore, most of the light beams will travel through the fiber core if there is a high contrast between the core and the cladding refraction indices. This statement is also proven by the concept of the numerical aperture

shown in Equation 3. A large numerical aperture of the fiber core indicates large ranges of angels at which light will be guided through the fiber core.

$$NA_{core} = \sqrt{n_{core}^2 - n_{cladding}^2} \quad (10)$$

where:
n_{core} is the refractive index of fiber core
$n_{cladding}$ is the refractive index of fiber cladding

Furthermore, the ray in Figure 6 gives the impression that there is no light propagation in the cladding under the TIR; however, the electromagnetic field penetrates to the secondary medium, as shown in Figure 8. The electromagnetic field decays exponentially from the surface of the boundary between the core and cladding regions. The electric field at the secondary medium varies with distance z normal to the interface surface by the following equation:

$$E(z) = E_0 e^{-\alpha z} \quad (11)$$

where
E_0 is the initial electric field at the boundary.
z is a distance at which the electric field is calculated
α is value varying with indicant angel, light wavelength, and indexes of refraction.

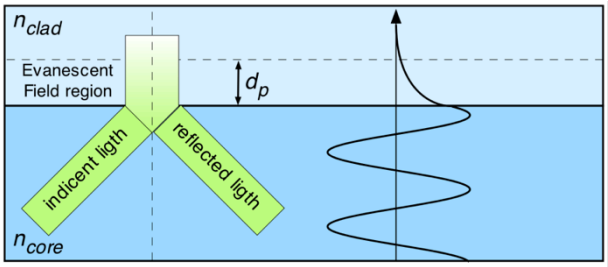

Figure 8 An evanescent wave decays exponentially in lower refractive index medium, Densmore *Sensitive Label-Free Bimolecular detection… 2008* [12]

Most of light energy is confined in the fiber core, and a small portion of the light energy propagates into the secondary medium, as shown in Figure 8. This field is known as the evanescent field (EVF). The length at which the EVF extends is called the penetration depth or d_p as shown in Figure 3. The penetration depth of EVF in an intact optical fiber is given by the following equation:

$$d_p = \frac{\lambda_0}{2\pi\sqrt{n_{core}^2 sin^2\theta_1 - n_{cladding}^2}} \quad (12)$$

where
n_{core} is the refractive index of the core.
θ_1 ,is the incident angle between the light beam and the normal.
$n_{cladding}$ is the refractive index of the cladding.

An important parameter that is needed in the study of the EVF is the V- parameter, which can give an insight of the number of modes a step index fiber can support as shown in the equation:

$$V = \frac{2\pi a}{\lambda_0} NA \quad (13)$$

where
λ_0 is the vacuum wavelength of the beam
a is the fiber core radius
NA is the numerical aperture

Having a V-parameter below 2.405 indicates that the fiber can only support one mode per polarization. In addition, the lowest order mode (LP_{01}) electric field can be approximated using *Gaussian beam.* Moreover, for $1.2 < V < 2.4$, the mode waist size w, shown in Figure 4, can ne approximated at a point in space where the electric field drops in a factor of 1/e using the following.

$$w \approx a(0.65 + \frac{1.619}{V^{1.5}} + \frac{2.879}{V^6}) \quad (14)$$

where
w is the mode waist size
a is the fiber core radius

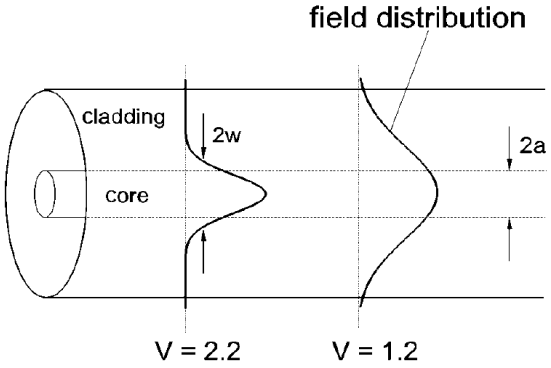

Figure 9 The relationship between the V-parameter and the mode waist size of evanescent field. Quimby, *Photonics and Lasers: An Introduction* [13](Quimby)

From Equation 14 and Figure 9 it can be determined that the V-parameter of the core decreases the mode waist size increases. To increase the sensing capability of the fiber, one needs to decrease the value of the V-parameter of the core to obtain large w/a ratio.

In the previous discussion, an intact single mode fiber waveguide was described. However, to use the EVF as surrounding medium sensor, one needs to reduce the fiber cladding and the core size so EVF will interact with the surrounding medium, which highlights the usefulness of a tapered single mode fiber. The process of fiber tapering involves removing a

large portion of the cladding, and elongating the fiber core, as discussed (below) in Section 4.3.2.1. When an optical fiber is tapered, the core V-parameter decreases as a result of the reduction in the fiber core radius resulting in a large portion of the mode to propagate outside the fiber core. As a large mode portion travels through the tapered section the mode goes through the adiabatic roughness and of the surrounding material causing the light to be scattered and lost before being transmitted through the core. One can detect changes in the light in the core using a photo-detector.

1.2.4 Data Collection Methods

1.2.4.1 Optical Fiber-Based Flow Rate Detection

A different detection technique utilizes the deformation of optical fibers inserted into the path of a microfluidic channel to determine the flow rate of the fluid. As demonstrated in *Microfluidic flow rate detection based on integrated optical fiber cantilever* by Lien and Vollmer [14], it is possible to determine a flow rate as low as 7 µL/min based on the transmission change of the optical fibers. In this experiment, a tapered single-mode fiber was inserted into the device to deflect with the passage of the fluid, as shown in Figure 10. A multimode fiber positioned in the wall of the channel receives the light from the single-mode fiber. Any change in the transmission corresponds to the deformation of the single-mode fiber, and therefore can be used to detect the flow rate. One problem with this method is that particles in the fluid could cause the fiber to deflect more, which would result in skewed measurements.

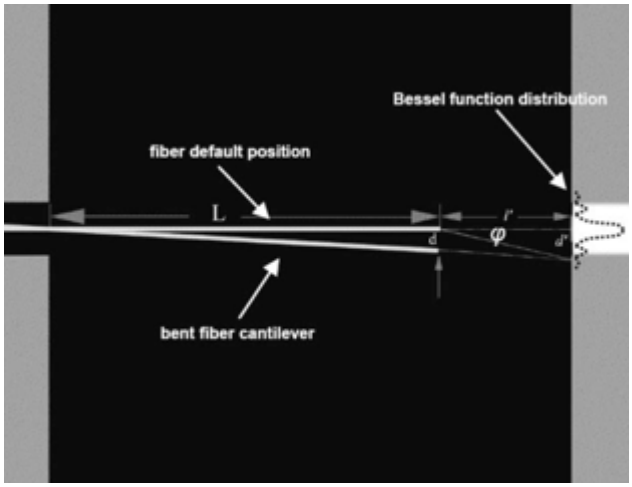

Figure 10 Approximate deformation of the optical fiber and intensity distribution of optical readout Source: *Lien and Vollmer [14]*

To determine the flow speed inside the microfluidic devices, one can suspend a fiber inside the channel that acts as a cantilever. When the flow rate increases, the embedded fiber is bent more due to the increased drag force. The deformation of fiber can be measured with a receiving fiber that collects the light from the other side of the channel. Victor, and Frank Vollmer presented microfluidic chip with fiber optics volume flow rate sensor [14]. The sensing mechanism relies upon the ability of fiber optics to bend. In the paper, Victor and Vollmer used

a tapered single mode fiber, (8.2 mm core diameter, SMFe-28 Corning) as a cantilever aligned with a multimode fiber (62.5 mm core diameter, CPC6 Corning), as depicted in Figure 11. As the fluid causes the cantilevered fiber to deform, the transmission received by the multi-mode fiber changes accordingly.

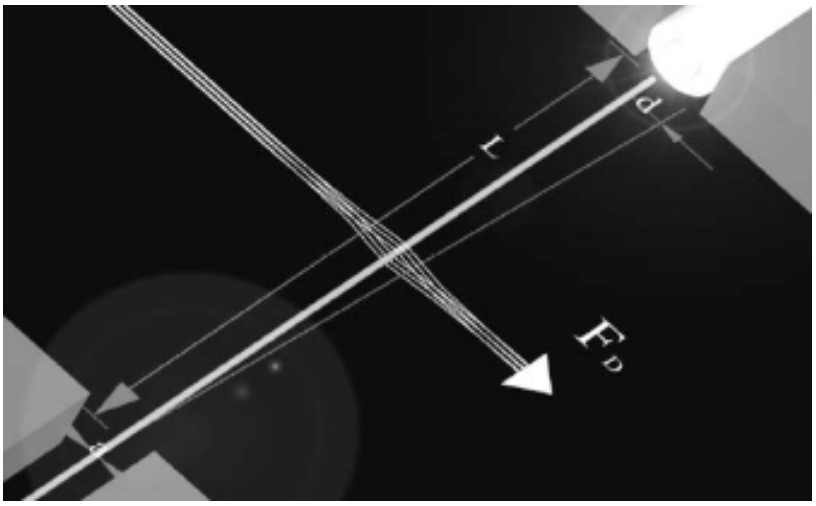

Figure 11 Integrated microfluidic flow sensor, Lien and Vollmer, *Microfluidic Flow Rate Detection…*(2007) *[14]*

1.2.4.2 Optical Imaging

Optical imaging of microscopic particles is typically performed with large microscopes and advanced equipment [15]. As self-contained technology such as Lab-on-a-Chip becomes more prevalent in analyzing microfluids and microscopic particles, a need arises to optically image samples without the use of expensive external micro-imaging hardware. Attempts have been made to image microfluids with comparable quality to a traditional microscope. "*Optofluidic microscopy—a method for implementing a high resolution optical microscope on a chip*" by Xin Heng et al [15] describes a method of imaging a sample by passing it over a series of skewed apertures (shown in Figure 12). By this method, light is transmitted from the top of the device onto a CCD camera to obtain a skewed image of the sample, which is then reconstructed. In order to reconstruct the image, the flow velocity must be known. This method has several more significant limitations; the imaging only works if the orientation and shape of the sample is unchanged. There is a screening process to identify cases in which the sample rotated and discard the corresponding data. Such filtering eliminates potentially useful data of a changing sample, highlighting the fact that this system is not robust for non-uniform fluid flows of varying shapes.

Another method called "lens-free tomography" uses a partially coherent light source to illuminate a sample from multiple angles to create several in-line projection holograms [16] (shown in Figure 13). This technology is limited by the scattering properties of the sample and experiences resolution loss if the sample is positioned too far from the sensor. Additionally, lens-free tomography requires the particles of interest to be stationary for the image collection, and makes a non-invasive trapping method for particles necessary. The limitations of such current optical imaging techniques demonstrate the need for a robust imaging system for microfluidic samples.

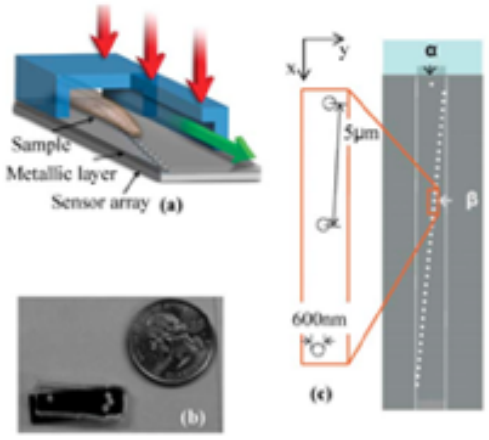

Figure 12 Optofluidic Microscopy, in which an image is assembled from a series of pinholes Source: X Heng, et Al. [15]

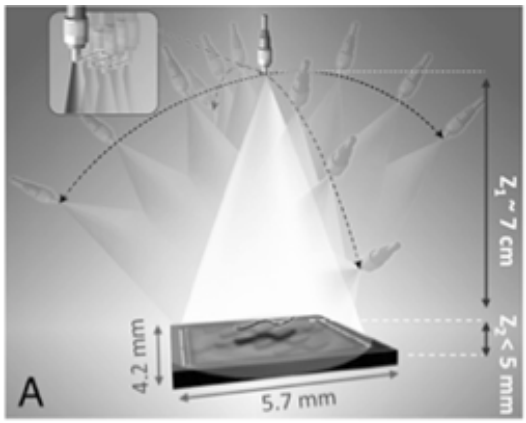

Figure 13 Lens-free tomography method of optical imaging from different angles Source: S.O. Isikman, [16]

1.2.4.3 Fiber Optics

Fiber optics is a growing technology for a range of applications for Lab-on-a-Chip technology, due to their size robust nature [17]. They can be used for a wide variety of sensors. Because optical fibers are composed of glass and plastic, they are impervious to harsh conditions and electromagnetic forces, making them ideal over common electronic sensors [18]. Studies have shown that fiber optics can be utilized in microfluidics for the optical tweezing of individual particles [19]. That is, light emitted from the ends of opposing optical fibers can suspend a particle in space or manipulate its motion. Multimode optical fibers and fiber bundles can also be used for imaging [20]. Fiber bundles utilize thousands of fibers bundled together to create a pixelated image, and can be up to a few millimeters in diameter. Multimode fibers have a relatively large core diameter that allows them to transmit a fluorescent image.

A group from the University of Arizona developed a system of imaging red blood cells on a Lab-on-a-Chip platform using a smartphone [21]. They developed a case to connect the smartphone to the microfluidic chip, utilizing waveguides that directed the image of the sample to the phone's camera, as pictured in Figure 14**.** The images of the red

blood cells were then analyzed using color detection features in commercial picture editing software.

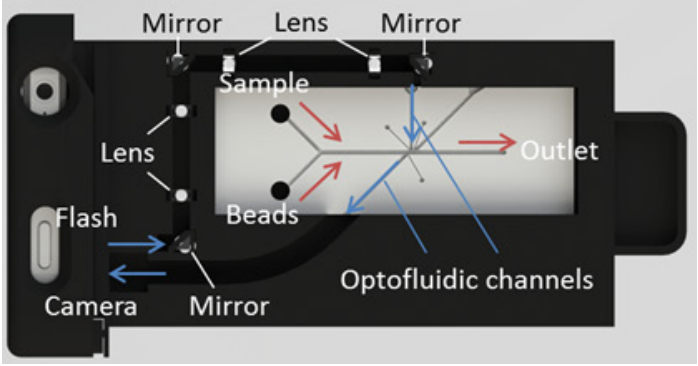

Figure 14 Smartphone-based Lab-on-a-Chip System , C. C. Stemple, et.al (2014). [21]

Another state-of-the-art optical imaging technique was recently developed by Pacific Northwest National Laboratory [22]. The researchers used glass beads less than 3 mm in diameter that offer up to 1000x magnification. They also created models for open-source 3D printed cases that can attach the beads onto smartphones or tablets for easy imaging of microscopic samples. This innovative and simple approach to small-scale imaging offers a cheap and portable alternative to traditional microscopes with little to no loss of image quality.

Nearly one fifth of the world's population uses smartphones, many for a variety of ever-increasing scientific applications [23]. Because of their high usage and prevalence in society, smartphones offer a common platform on which the general public can gain access to advanced scientific analysis. Therefore, smartphones would be very advantageous tools to use if Lab-on-a-Chip technology were to become widespread on commercial level.

1.3 Challenges

One of the primary challenges of this project is that the mechanical engineering department of Worcester Polytechnic Institute currently has no formal procedures for integrated, mechanical, micro-fluidic device research. A significant portion of this project includes the development of such methods. A challenge of Lab-on-a-Chip in its current state is the lack of commercial components to be used in a system. [4] Researchers tend to develop specific parts for their own applications, as with any new technology.

1.4 Scope of Work

The current state of microfluidics highlights a need to make the technology more user-friendly in order to expand its availability to a variety of users. The work of this MQP, which will be described in the rest of this paper, combines the novel techniques used in each of these areas into a self-contained, modular, and integrated lab-on-a-chip device that would be user friendly. The design utilizes a self-pump system to drive the fluid motion, a fiber-optic-based flow detection system, and a smartphone-based imaging system. Such a design is also adaptable so that additional modules, such as a spiral-channel separation system,

could be added to the system easily. Moreover, an efficient fabrication process for microfluidic devices using novel techniques was developed. Such procedures are valuable to research with limited access to full fabrication resources or whose research does not rely on proper clean-room procedures but rather the establishment of a simple micro-mechanical system. The rest of the paper is organized in the following manner: The device designs will be discussed in Section 2. Section 3 describes the methods used to fabricate the devices for testing. The results of the tests will be detailed in Section 4, followed by discussion in Section 5.

2. Design

The goal of the project is to have a Lab-on-a-Chip system that can pump the liquid carrying the samples, separate the samples, and retrieve data from the samples. For experimentation, these separate functions of the system were divided into the following four isolated modules: Smartphone-based imaging system, Particle separation device based on Spiral Design, Self-powered pumping device, and Optical fiber drag force sensor. Each of these modules was isolated to be tested separately, with their combination and integration into a single device being the end goal.

2.1 Smartphone-based Imaging Device

The smartphone microscope technique developed by Pacific Northwest National Laboratory [22] was used to image the microscopic particles using a smartphone and glass beads. Up to 1000x magnification is possible using their designs. However the 100x magnification option is sufficient for Lab-on-a-chip imaging. First, the clips to hold the glass beads, shown in Figure 15, were 3D-printed using the open source .stl files posted on the PNNL website [24].

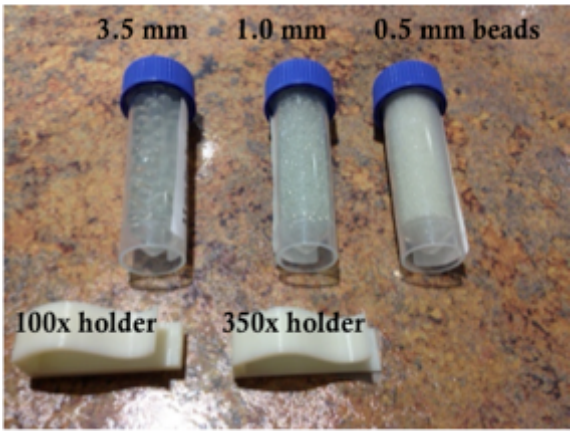

Figure 15 Glass beads and holders used for smartphone microscope

Several different channel designs were created to test the imaging of microfluidic particles in a Lab-on-a-Chip system. The patterns, shown in Figure 16, have a variety of channel sizes and shapes to test the ability of the imaging system for different flow rates and channel widths. Each of these patterns was also made with a thin channel perpendicular to the flow (shown in Figure 17) into which an optical fiber could be inserted for measurement of a fluid's concentration.

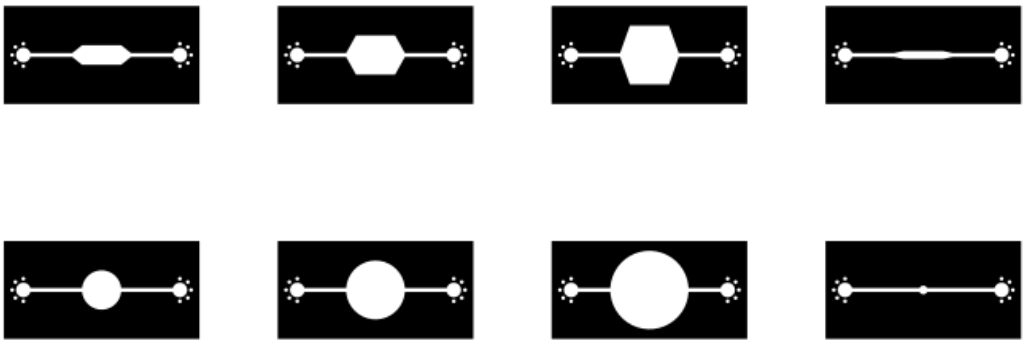

Figure 16 Multiple channel designs for imaging

Figure 17 Imaging device with groove for optical fiber

The pattern shown in Figure 18 is a new design for trapping micro-particles for imaging. By using the T-shaped tab design, particles in a fluid solution would flow in through one of the input channels on the left and get trapped by the T-Shaped tabs in the center of device, shown expanded in Figure 18b, so that they can be imaged in a stationary position. Once the image is taken, the flow in the first input channel would cease and flow would be turned on in the second channel. This secondary fluid flow would clear the trapped particles out of their T-shaped trap and push fresh particles into the traps to be imaged. This design was made using two different sizes, 15 um and 25 um, for the walls of the T-shaped tabs.

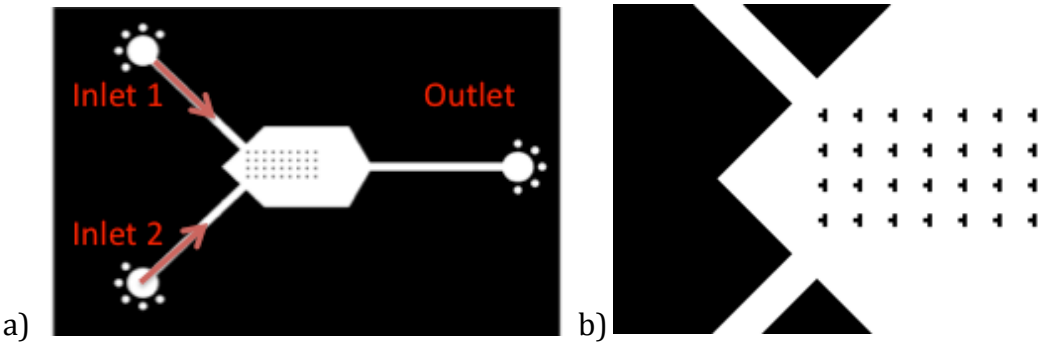

Figure 18 a) T-shaped tab catcher design, utilizing two inlets to trap particles for imaging b)Magnification of T-shaped tabs

2.2 Particle Separation Device based on Spiral Channels

Based on the literature, single spiral [7] and double spiral channels [8] can serve as sample separation modules for the final Lab-on-a-chip system. The Dean and Reynolds numbers vary with the channel dimension and the curvature of the channel. Two groups of designs were created, as shown in Figure 19. The first group of designs consists of a double spiral channel with one inlet and two outlets shown in Figure 19a. In the double spiral design the fluid rotates from the inlet channel through the S-shaped junction and is then divided into two outlets. Though not crucial to the functionality, the S-shaped junction connects the first and second spirals, resulting in the final double spiral. The second design shown in Figure 19b is a single spiral channel that contains one inlet in the middle of the design and then rotates to end in two outlet channels Six variation of each group was created, based on the height, width, curvature, and the pitch of the spiral channel. Having different designs with different parameters allows one to determine which features are most important for separation.

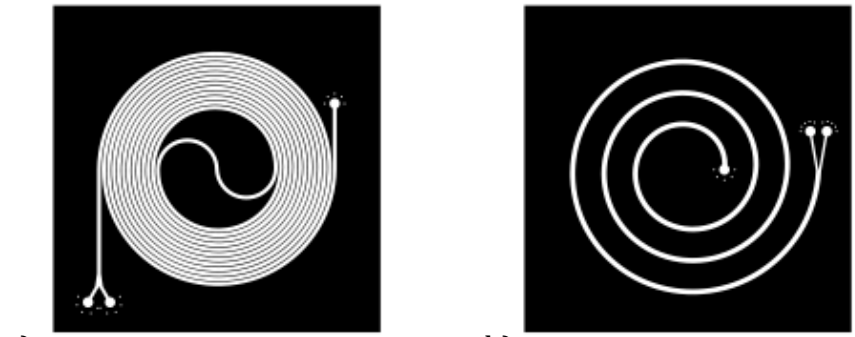

Figure 19 Shows the different design groups for the separation module. a) Double spiral designs, in which the flow starts and ends outside of the circle, b) single spiral design, in which the flow starts in the center of the circle and leaves on the outside.

2.3 Self-Powered Pumping Device

The designs for the self-powered were based on those implemented in *Self-powered Imbibing Microfluidic Pump by Liquid Encapsulation* by Kokalij et al. [6] The only differing factor was the angle of the fan, shown in Figure 20, which has an effect on the fluid flow rate. Once the devices were fabricated by the procedure described below, filter paper would be cut to fit into the fan area.

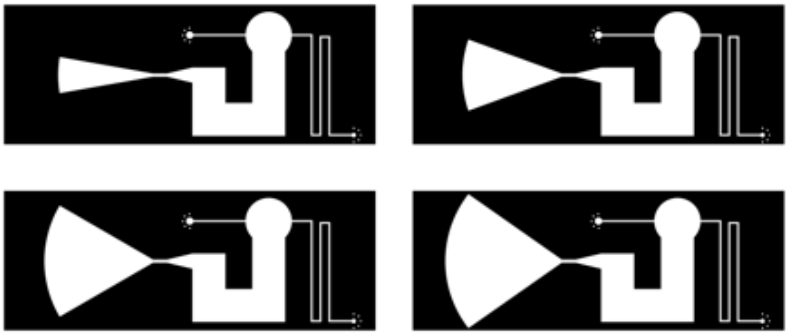

Figure 20 Four different pump designs varying the pump size

2.4 Drag Force Measurement Device with Embedded Optical Fiber Taper

The literature [14] suggests that an optical fiber can be inserted into the channels to obtain data from the moving fluids. There are two methods of inserting a fiber into a device: by lowering the fiber onto the device or by raising the device up to the fiber. For a fixed positioned device, two tapered fiber were created. The first is a straight and the second is bent. A tapered fiber was bent and U-shape fiber was created. The reason for this U-shape fiber is to decrease the fiber movement from the ambient air motion while inserting. In addition, having the PDMS fixed increases the probability of not breaking the fiber. As a result of these insertion methods and the type of the tapered fiber, four main designs were created.

The first design, shown in Figure 21a, involves two wells that are positioned perpendicular to the fiber channel. The wells were added to glue the fiber during insertion. However, it was found that gluing the fiber close to the tapered region caused significant transmission loss. As a result the second design shown in Figure 21b was created. This design has a long channel for the fiber, so that glue can be applied far from the tapered fiber waist. This channel is fairly wide so that the fiber does not break the channel edges. The third design shown in Figure 25c was made to insert a U-shaped fiber without restricting the width of the U-shape as in Figure 21a. The fourth design shown in Figure 21d was created in order to give the fiber large space to deform in the presence of a flow.

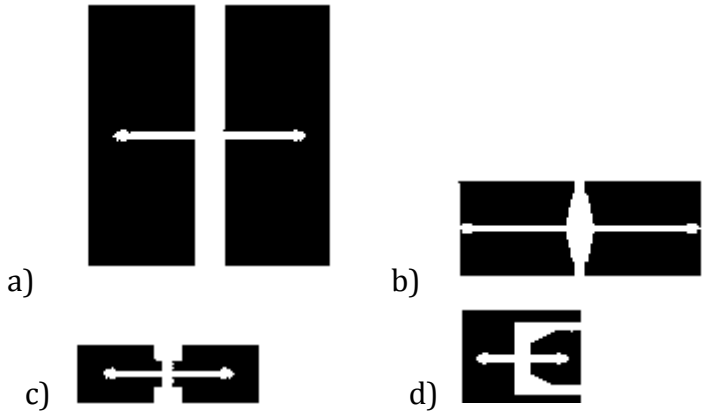

Figure 21 Device Designs for Embedded Tapered Fiber

2.5 Overall Design

Designs from each of these categories were selected to be part of the final design of a single, stand-alone, modular device that integrates a self-powered pump, utilizes optical fibers as a flow sensor, and images microscopic particles on an accessible user interface. This final design is shown in Figure 22. Each of the components of this design is discussed in more detail in Section 4.

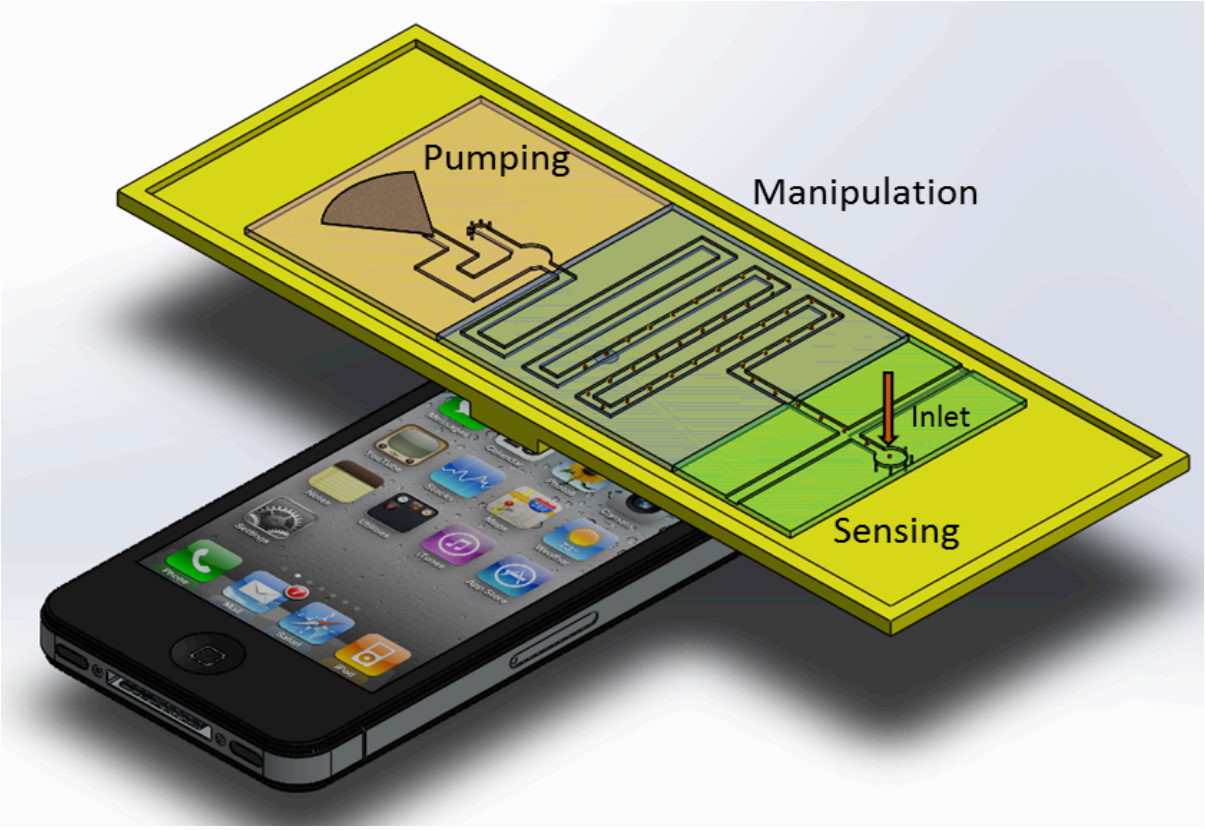

Figure 22 Final Design of the integrated system featuring a self-powered pump, sample manipulation module, optical fiber based drag sensor, and user-friendly imaging platform.

3. Fabrication

Several different methods were used to fabricate the devices for testing. As the project evolved, some traditional methods proved too inefficient for the time and resources the team had available. Newer faster methods were tested and utilized that met the needs of the team to fabricate devices quickly for mechanical testing.

3.1 Traditional Method

The microfluidic devices were fabricated using soft-lithography with SU8 master molded on silicon substrate with a layer of photoresist. By this subtractive photolithography method, ultraviolet light passes through the exposed areas of a photo-mask mask to dissolve photoresist on a silicon wafer, leaving the desired pattern etched on the wafer, as shown in Figure 23. Typically, the designs for a microfluidic device are rendered in AutoCAD and sent to a company called CADArt for printing on a transparent sheet used as a photo-mask. This procedure could take 1-2 weeks for the company to process and deliver the photo-mask.

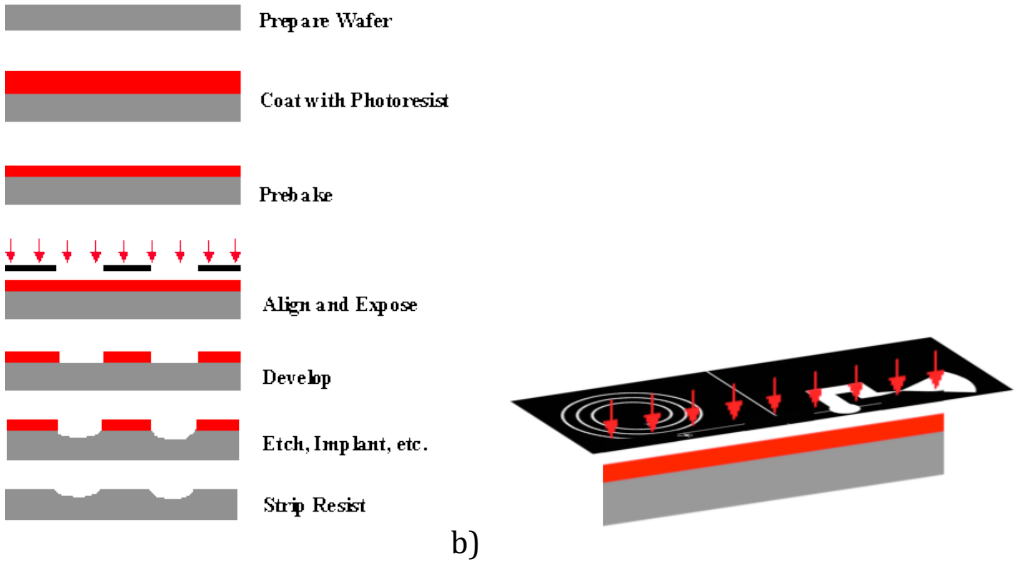

Figure 23 a)Standard soft lithography process, Source: C. A. Mack [25] b) Example of a device design being etched onto a silicon wafer for fabrication

Once the silicon wafer and photo-mask had been obtained, a small container was lined with either foil or plastic or some sort of lining that can be molded to fit the container. The type of container will depend on which method the user decides to use: the baking method and the traditional method. The next step was the mixture of the liquid PDMS and the bonding agents. The amount of PDMS to bonding agent followed a 10:1 ratio. For this project, 30 mL of PDMS was mixed with 3 mL of the bonding agent and poured into a 75 mm dish 5mm deep, coating the silicon wafer. When mixed, the substances resemble a bubbled liquid, as shown in Figure 24.

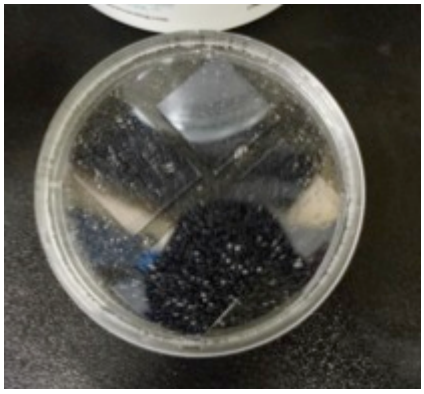

Figure 24 Bubbled PDMS in liquid form on wafers

By this method, either a glass or plastic container could be used, as long as the container has a cover to keep the device clean. The device is then left in a flat stable environment in order to cure properly. The air bubbles caused in the mixture would rise naturally as time passed and become clear. This curing process typically took 2-3 days, and was best used if the user was not working under tight time constraints. Once the devices cured, they were cut out using a small blade. A biopsy punch like the one shown in Figure 25 was used in order to create openings for both inlets and outlets. It is very important that this puncher be the correct type for the PDMS. This certain type of puncher not only pierces through the whole device, but also removes any PDMS leftovers that might cause clogs or close off the channels and prevent flow from entering the device.

Figure 25 Fabricated PDMS Device with inlet/outlet holes being punched with a biopsy punch

Next, the PDMS devices were bonded to a substrate in order to seal the channels. The most common way to bond PDMS to glass is using an O_2 plasma treatment, which oxidizes the PDMS surface so silanol groups (-OH) are developed. [26] The silanol groups make the treated PDMS surface highly hydrophilic. When an O_2 plasma treated PDMS surface is brought into contact with a treated glass surface, the silanol groups on both surfaces condense with each other and yield Si-O-Si bonds by losing a water molecule. This covalent Si-O-Si bond forms a strong irreversible seal between the PDMS and glass. [26] However, this requires an O_2 plasma machine and special training. Even when properly trained, bad bonding could frequently occur.

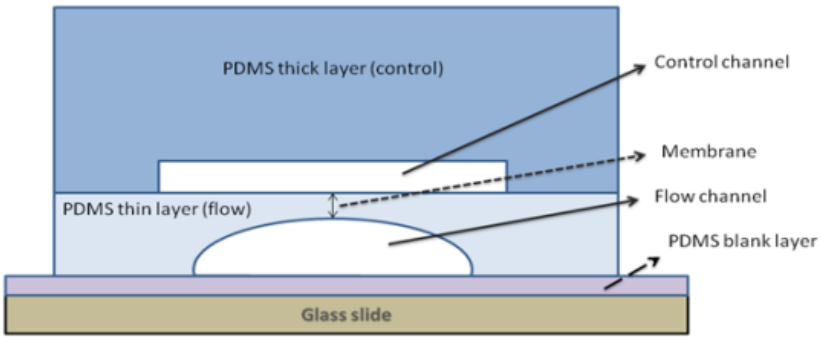

Figure 26 Diagram of the traditional bonding of a microfluidic device, Bhattacharya et al, *Studies on Surface Wettability of Poly(Dimethyl) Siloxane (PDMS) and Glass…* 2006 [26]

3.2 New Fabrication Techniques

3.2.1 Self-Printed Photo-masks

To reduce the time spent receiving photo-masks from a company, the team experimented with masks fabricated using a home printer and commercially available transparency sheets. Of several printers tested it was determined that color laser printers created photo-masks of the best quality. The limiting factor of this method was the resolution limits of the printer, which was far less precise than the professional printing. Nevertheless, devices were successfully fabricated using these self-printed photo-masks. Although the channels of these devices often had a jagged edge compared to the professional printers (seen in Figure 27) they bonded and passed a fluid as sufficiently as devices fabricated with the traditional method.

a) 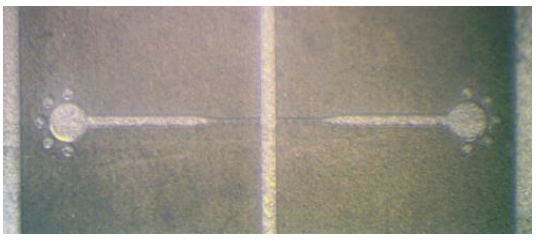 b) 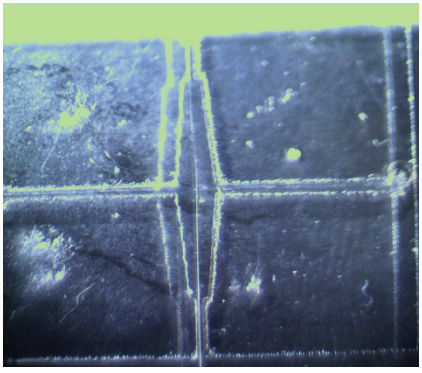

Figure 27 a) Standard resolution of a device fabricated using a professionally printed photo-mask. b) Jagged edge of a device fabricated using a self-printed photo-mask. Despite the lower edge quality, the latter device functioned as well as the device in Figure 27a.

3.2.3 Heated Curing of PDMS

Heated curing was a technique that helped the team to significantly decrease the waiting time in regards of preparing the PDMS [27]. Rather than wait a few days for the PDMS to settle and cure, this heated curing method reduced the process from days to hours. For this method, a glass container should be used and an oven will be needed. If an oven cannot be

accessed, a hot plate covered with a box, like the one shown in Figure 22 can be used as a substitute. A vacuum chamber like the makeshift one shown in Figure 23 may also be used to make the process smoother and faster.

Figure 28 Hot plate that was used; box was placed over it to create an oven-like atmosphere

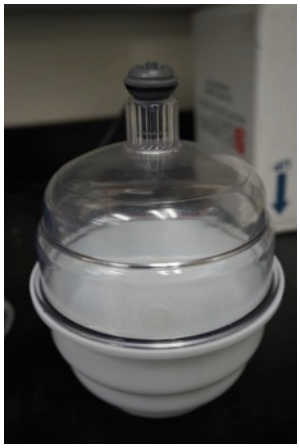

Figure 29 Vacuum chamber obtained from Bel-Art Products, sealed using makeshift techniques involving a wine stopper

When the mixing of the PDMS and bonding agent occurs, multiple air bubbles will form within the mixture. Waiting for the bubbles to naturally rise would normally take about a day. The team found an alternative method that would reduce that waiting time to 10 minutes. The vacuum chamber is easy to use and only requires a pump in order to vacuum out. This method greatly speeds up the curing process.

Once the PDMS has been cured, it is placed in the vacuum chamber to depressurize it. This process removes almost of all the air bubbles. The sample is then placed in the oven or makeshift oven for 2-3 hours at 165 C to cure.

3.2.2 Tape Bonding Method

An alternative, inexpensive bonding technique that does not rely on special equipment is the tape method. For this method, researchers found that tape and an oven can be used to create bonding between the PDMS and glass [28]. The tapes have varying properties and hence yield different bonding quality. Certain types worked better than others, and

different tape brands would work better with certain designs. The tape was placed between the PDMS and the slide with the sticky side against the PDMS, and the device was pressed together firmly to ensure that no air bubbles are caught in the device. The oven is heated to 165 C. The device is then placed into the oven or plate and box and left to bake for approximately 2 or 3 hours.

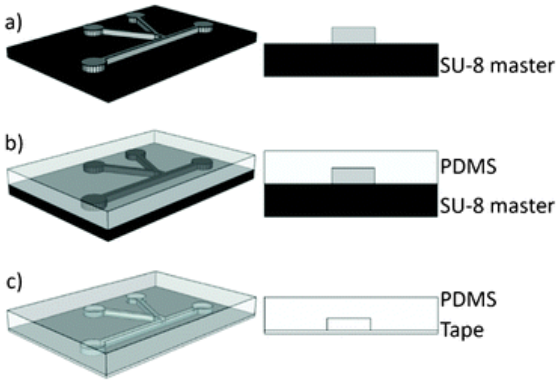

Figure 30 Fabrication steps for Tape Bonding. After device pattern is imprinted on the PDMS, the device is bonded to a tape substrate instead of the traditional glass [21]

A comparison of the traditional method and, new tape bonding method is shown in Figure 31.

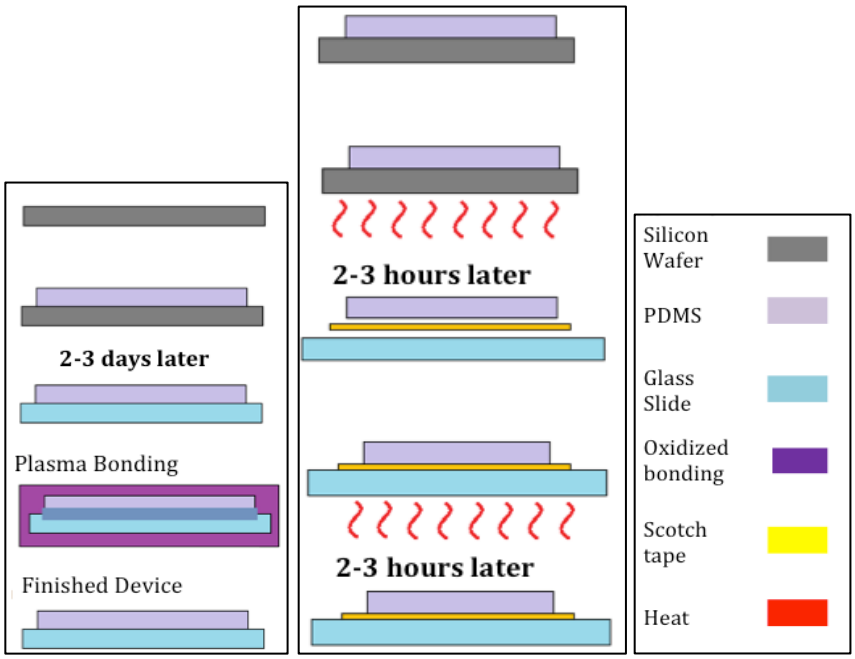

Figure 31 Schematic of the fabrication methods a) traditional b) new

4. Results

4.1 Simulation

Simulation of the fluid flow through these device designs was run in COMSOL Multiphysics, which utilizes the finite element method. Figure 32 shows the results of one such simulation of the dual-input design without the T-shaped patterns. The velocity magnitude of the simulation behaves as expected, with a greater velocity in the single outlet channel. Once the T-Tabs were added to the model, the velocity profile became more complex, as shown in the velocity contour plot with streamlines shown in Figure 33.

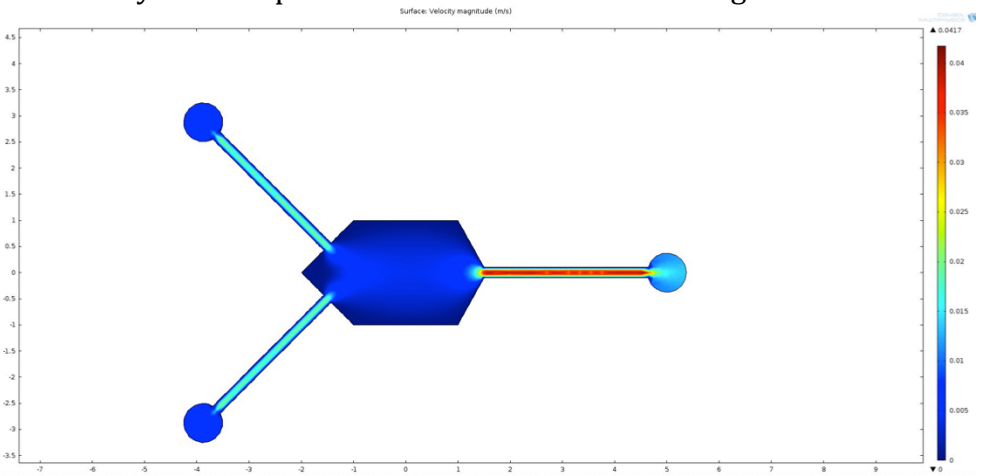

Figure 32 Velocity magnitude of a fluid flowing through a dual-input device without T-shaped tabs. The COMSOL simulation agrees with expected outcomes.

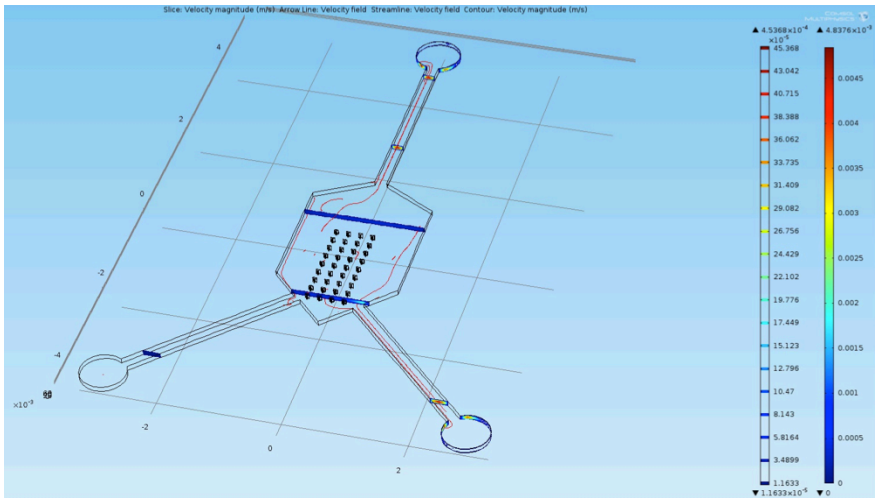

Figure 33 Velocity profile cross-sections with streamlines for a device with T-shaped tabs. The complex geometry makes the velocity profile more complex, as expected.

As described in later sections, leakage out of the optical fiber channels became an issue that significantly affected the fluid flow through the device. A simulation was run of a circular imaging device to understand the impact of this leakage on the fluid velocity. The results of this simulation are shown in Figure 34. In this model, significant leakage occurs out of one

of the fiber channels, which significantly reduces the flow through the intended outlet of the device.

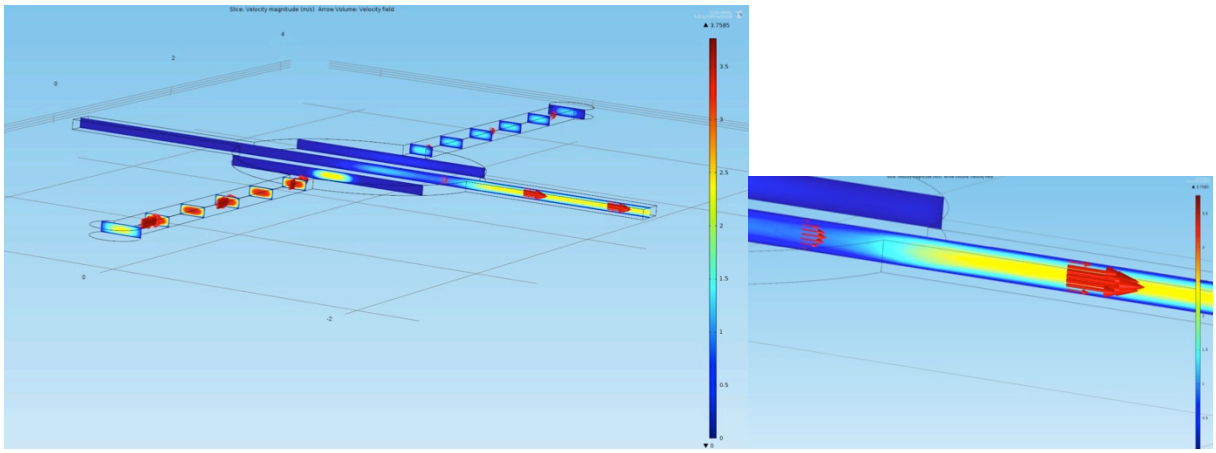

Figure 34 a) Cross-sectional velocity profile of fluid flow through a circular imaging device with leakage out of an optical fiber channel. As the close up on this channel in (b) shows, the majority of the fluid flow leaves through this channel, while the flow is greatly reduced in the intended outlet.

This successful simulation illustrates the expected behavior of fluid flow through the design microfluidic devices for imaging.

4.2 Cell-Phone-Base Imaging

The clips designed by Pacific Northwest National Laboratory [22] for a smartphone microscope were fabricated using a Dimension SST 1200ES 3D printer. The holes to hold the imaging beads were found to have been printed slightly smaller than the beads themselves. This discrepancy was likely due to differences of 3D printer tolerances in addition to potential shrinkage of the ABS plastic as it cooled. In order to properly hold the beads, these holes were drilled out using a 9/64-drill bit for the 3.5 mm beads and a #56 drill bit for the 1.0 mm beads. Once the beads were secured in the clips, they were attached to an iPhone 4S, as shown in Figure 35. Preliminary tests with text on a paper yielded clear results of the device, as shown in Figure 36.

a) 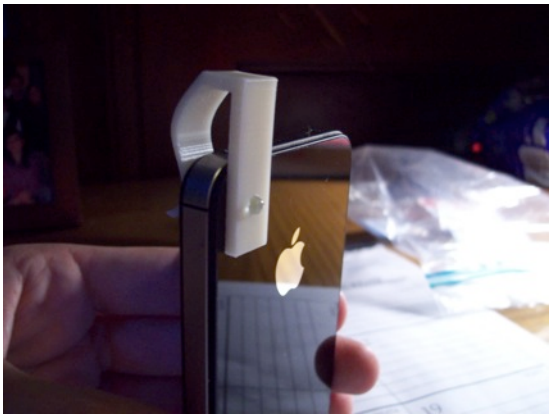 b) 

Figure 35 a) 3D-printed plastic clip with bead affixed to iPhone 4S. The bead protrudes from the clip because the hole was printed slightly smaller than it should have been. b) close up image of the microscope bead clip

a)  b) 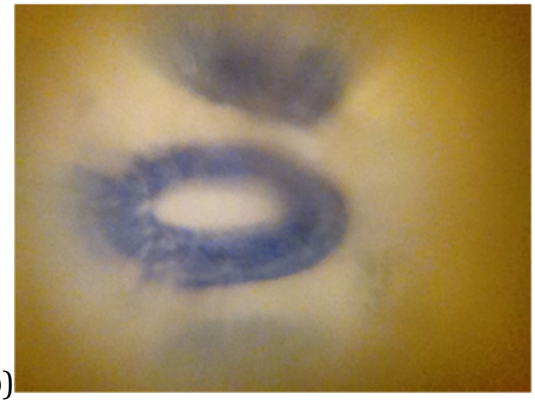

Figure 36 a) Preliminary testing results of imaging writing on paper with 100x magnification b) The resulting image from the iPhone of this imaging test.

Next, tests were conducted to image a sample of red-dyed water passing through a microfluidic channel. Figure 37 shows the clear imaging of this channel taken with a cell phone. 100x magnification was sufficient to view microfluidic flow with a cell phone.

a) 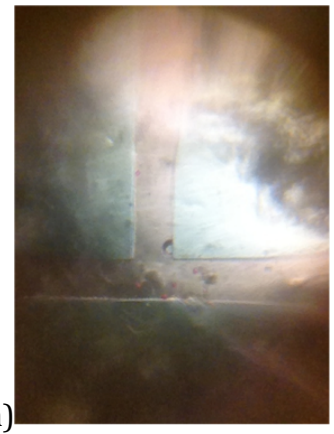 b) 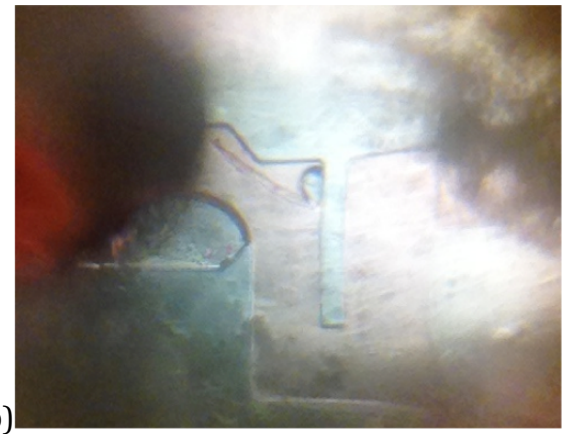

Figure 37 a) Clear imaging with cell-phone microscope of red-dyed water passing through a microfluidic channel b) a different portion of the same microfluidic device, including inlet pipe on the left.

The optical aberration on the edges of images taken with the smartphone is due to the curved glass bead used to magnify the images for the smartphone camera. Higher magnification with smaller beads is possible as previously mentioned. However the aberration is also greater, and restricts the field of view.

A diluted solution of red 15 um beads was passed through several of the device designs described in Section 2.1 for testing of this imaging system. Due to problems with the bonding, the large cavity in the center of the device did not fill with fluid as intended. However, fluid was able to flow around the edges of the chamber as can be seen in Figure 38a. This image was taken with a standard stereomicroscope. Figure 38b is an image of the same system taken using the smartphone with the 100x magnification bead. As a comparison between these two figures shows, the images taken on the smartphone are of comparable quality to those taken with the stereomicroscope.

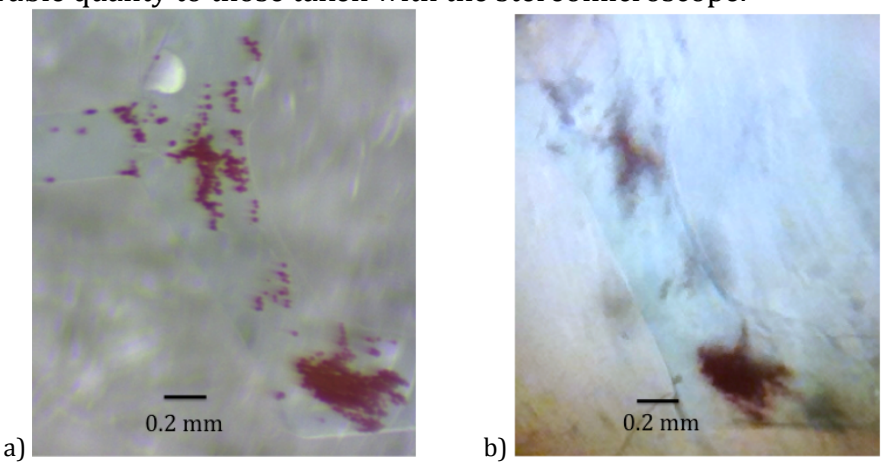

Figure 38 a) Magnification of the microfluidic device using a stereomicroscope. Despite issues with the bonding, the fluid passed through the device sufficiently enough to image the microscopic particles b) Image of the same device taken with a smartphone, with quality comparable to that of the stereomicroscope.

Some of the blurriness of Figure 38b is a result of a poor user interface. With the current design of the smartphone clip, it is not possible to lay the phone flat with the microfluidic device placed securely on top of the imaging bead. In order to take a picture such as that in Figure 38b, the user must hold the glass slide with the device while taking the picture on the phone and operating any other lab equipment in the area to control the fluid flow. Such a practice highlights the need for a better securing method of the microfluidic device while image.

In response to this need, a plastic holder shown in Figure 39 was designed to secure the device flat on the cell phone. This holder allows the device to be positioned freely to align the area of interest with the phone camera, and allows the user freedom to image the sample more precisely.

a)  b) 

Figure 39 a) Holder 3D printed to secure the device in place while imaging b) attached to cell phone

4.3 Optical Fiber-based Flow Detection

As reviewed in Section 1, fiber optics can be a valuable component of a lab-on-a chip. Because of their robustness, the team tried several different methods to integrate fiber optics with the microfluidics devices. The fibers in the microfluidic device can be deformed by the drag force from the flow passing the fiber and hence serve as a flow sensor. The detection methods that the team investigated to measure fiber deformation are 1) optical power transmission monitoring using two separate fibers (one receiver and one transmitter) and 2) optical imaging of a single deformed fiber taper.

4.3.1 Transmission Measurements between Two Aligned Fibers

Optical fibers were inserted in the devices by means of a three-dimensional translational stage. The device would be fixed with the features face up, while the optical fibers would be precisely positioned using the stages and secured to the device using glue. Figure 40a shows two fibers in the process of being aligned, while Figure 40b shows two successfully aligned fibers in a device.

a) 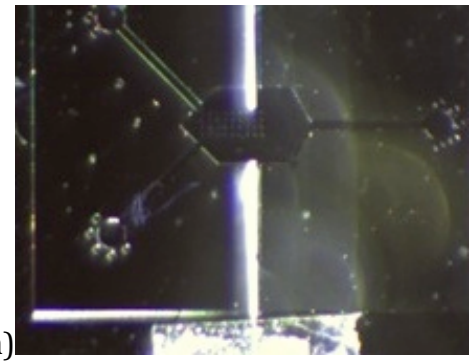 b) 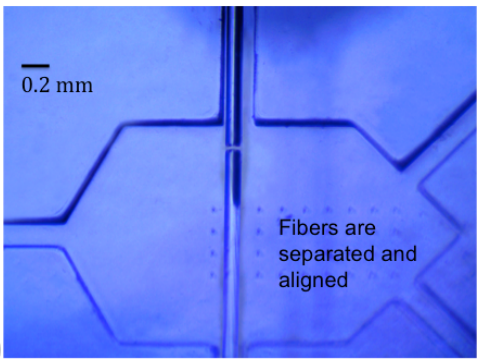

Figure 40 a) Two optical fibers in the process of being aligned b) Successfully aligned optical fibers in a device

Once two opposing optical fibers were successfully inserted into the device, the optical transmission from one fiber to the other was measured. The deforming fiber is connected

to a laser source and the fixed fiber to a photodiode. When the system is at rest, light propagates through source fiber and is collected by the fixed optical fiber. When the source optical fiber deforms, he receiver fiber receives less optical power. The change in optical power through the receiver fiber can be measured with a digital instrument and used to determine the deformation of the fiber, and therefore the flow rate of the moving fluid. Unfortunately the team was unable to measure any transmission in these tests. One reason might have been that the tips of the source fibers may not have been cleaved properly. Additionally, the deforming fiber may have become stuck to the PDMS, losing the light to the device rather than the receiving fiber.

4.3.2 Measuring Deformation Visually

Because the two-fiber method was challenging due to poor control of the fiber diameter and small microfluidic channel width, the team decided to measure the deformation of a single fiber taper visually using a camera. This method would be easily integrated with the smartphone-based imaging platform.

4.3.2.1 Fiber Tapering Process

That basic principle of fiber tapering is to remove large portion of the fiber cladding in order for the EVF to extend to the surrounding medium. This is often done by heating and pulling an optical fiber. Yundong Ren, a PhD student in Mechanical Engineering at WPI, developed the fiber tapering method used for this project. This tapering mechanism involves two motorized translation stages and a stationary propane torch. The two translation stages hold the optical fiber and move it over the flame while applying tension to the fiber. This process allows one to have narrower fiber diameter, which can be used for sensing applications. A schematic of the fiber tapering process and a picture of the procedure are shown in Figure 41Figure 42, respectively, courtesy of Yundong Ren.

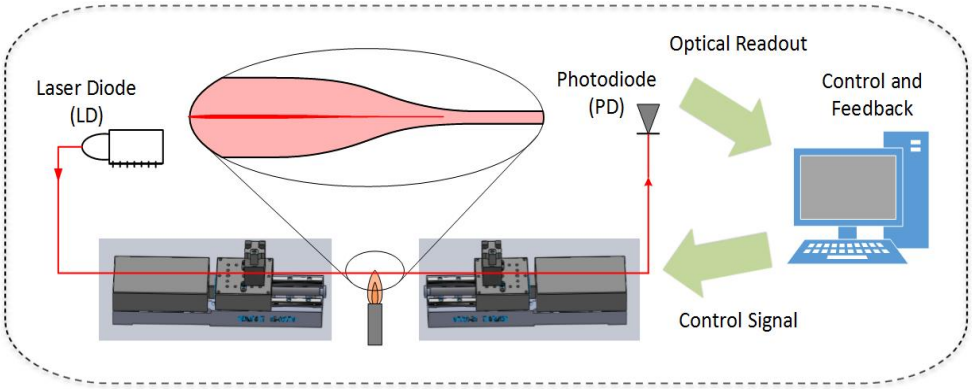

Figure 41 Schematic of the fiber tapering process, including heating and drawing, with the even pulling speed being controlled by a virtual instrument. Courtesy of Yundong Ren

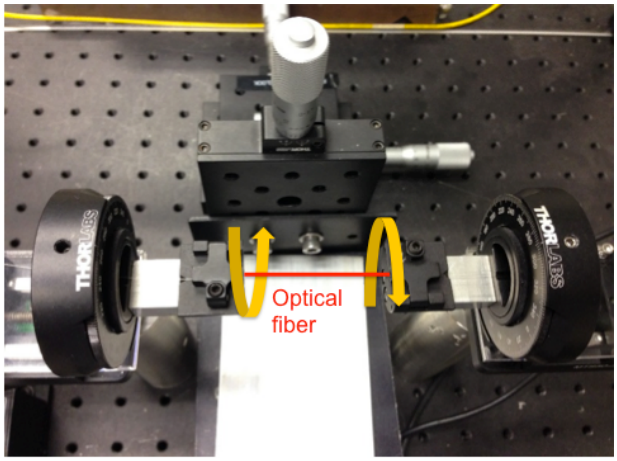

Figure 42 Image of fiber being tapered, courtesy of Yundong Ren

4.3.2.3 Testing of Tapered Fibers as Flow Sensors

A fiber with the polymer buffer stripped, a tapered fiber with a broken tip, a U-shaped fiber taper, and a straight fiber taper were fabricated and tested, as shown in Figure 43 and Figure 44. Once these fibers were prepared, they were inserted into a microfluidic device. For the fibers shown in Figures 41 and 42a, b, and c, this was done by lowering the fiber by mean of a three-dimensional translational stage onto the feature side of a fixed PDMS device prior to bonding. The unbroken, unbent tapered fiber shown in Figure 123D was inserted by raising the PDMS device on a translational stage to the fixed and freshly tapered fiber, in order to avoid breaking the narrow fiber.

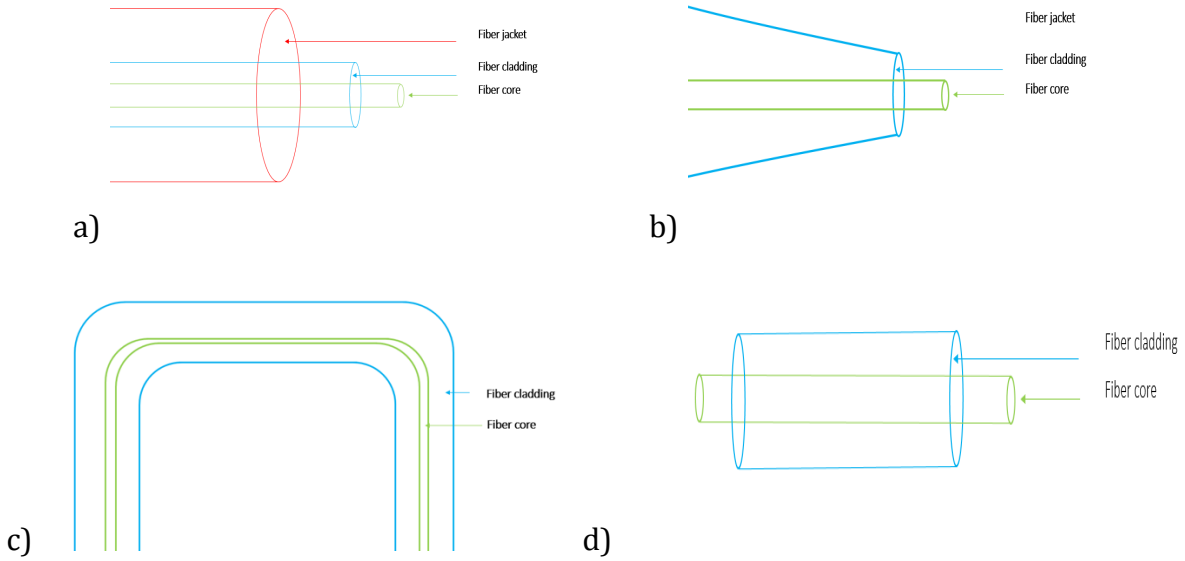

Figure 43 Schematics of a) a stripped fiber b) a broken tapered fiber c) a U-shaped tapered fiber d) an unbroken tapered fiber

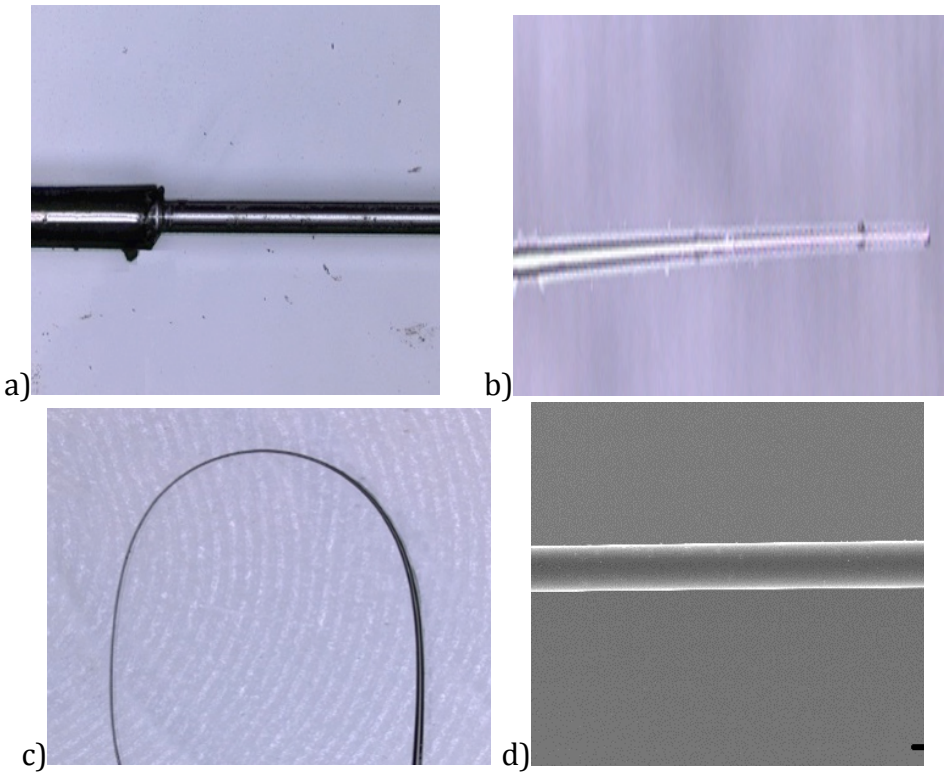

Figure 44 Images of a) a stripped fiber b) a broken tapered fiber c) a U-shaped tapered fiber d) an unbroken tapered fiber

Once a fiber was successfully aligned in the fiber groove as shown in Figure 45, it was glued to the device away from the features and in most cases, beyond the tapered region of the fiber. This gluing was performed more easily on devices that were designed with glue points, such as those shown in Figure 16 (pictured below). The broken tapered fiber tip was difficult to install because it would vibrate and could easily get stuck to the channel walls. The U-shaped fiber taper was more stable while being installed, but required either a device with a small width or a specifically designed device with a U-shaped groove. As Figure 46 shows, excess glue on the device makes the device surface uneven and causes problems when trying to bond the device.

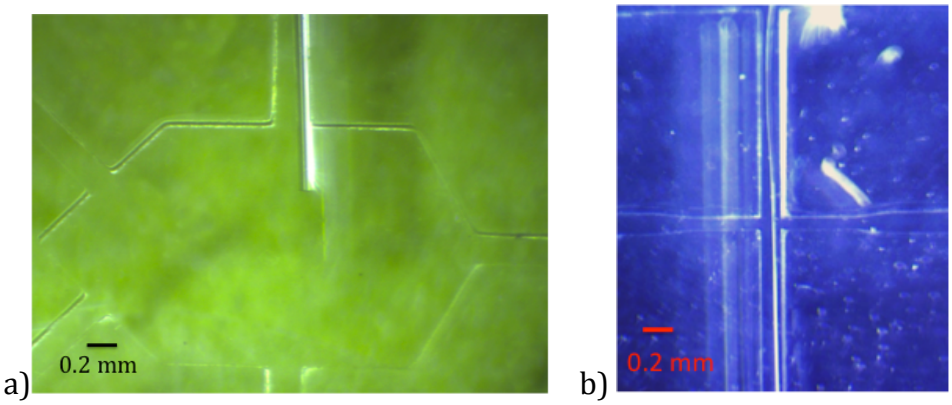

Figure 45 Successful insertion of broken tapered fibers into devices

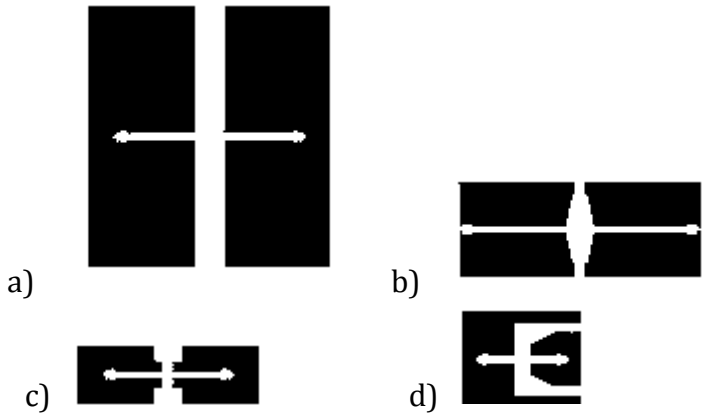

Figure 16, for reference Device patterns designed for the purpose of inserting and securing tapered fibers without losing transmission due to the glue points.

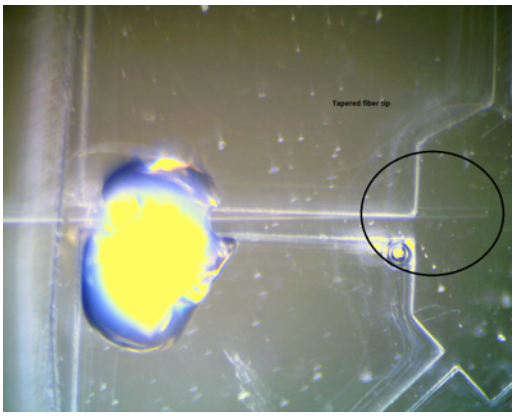

Figure 46 Excess glue used to secure the fiber could make the device uneven

After the glue dried, the device was bonded to a tape substrate by the procedure described in Section 3.2.2. Care had to be taken to avoid damage to the fiber in the oven. Devices that boned successfully were used for flow testing to observe deformation.

It was difficult to observe deformation of the tapered fiber because it was barely visible under the regular stereomicroscope, especially with the water flow in the channel, due to its small width (1~3 micrometers). Moreover, fiber deformation was not observed nor captured with a camera with the flow rate of 25 ml/m. The fiber tip was likely stuck to the bonding tape or the ground layer of the PDMS.

In order to solve this issue, tapering a fiber using hydrofluoric acid (HF) might be better than the drawn while heating method, since the fiber polymer jacket can be used to insure that the fiber tip will not stick to the surrounding sidewalls. A typical HF-etched optical fiber is shown in Figure 44. Another method that can fix this issue is to use a tapered fiber with a shorter taper length, which can be future work for improvements.

4.4 Self-Powered Pump

4.4.1 Results

In an attempt to make the device more stand alone, the concept of a self-working pump was integrated into the final design.

The primary concept was to create a pump that did not require any outside equipment, as shown in Figure 47. Normally, microfluidics would use a mechanical pump to initiate flow within the device; this also allowed manipulation of the flow with exact numbers. However the original idea behind LOC is to reduce the use of lab equipment, hence why this concept was deemed worth pursuing.

The only setup that the device requires is a prefill so that the device can be activated when it is needed. The larger channels are filled with a liquid up until the fan opening. Once it is in place, another liquid can be placed on the test channel inlet and the testing can begin. The only thing that is needed to activate the pump is the simple press of a finger. The flow should begin to initiate once the liquid makes contact with the porous material. Numerous tests were done in order to find the ideal bonding strategy. A small short flow was obtained during one of these tests shown in Figure 48, which proved that the concept worked.

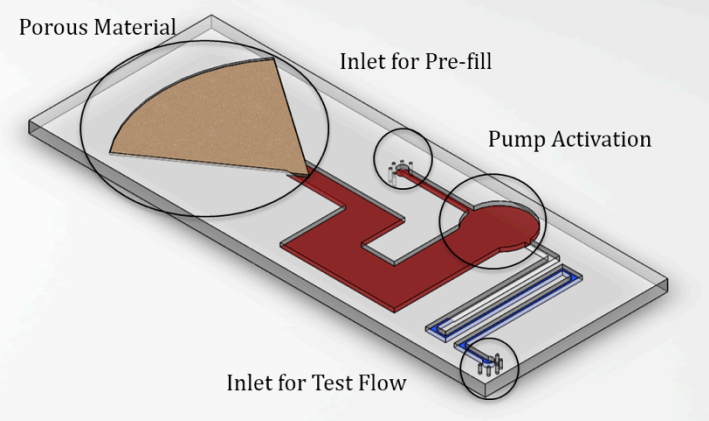

Figure 47 Schematic of self-pumping system

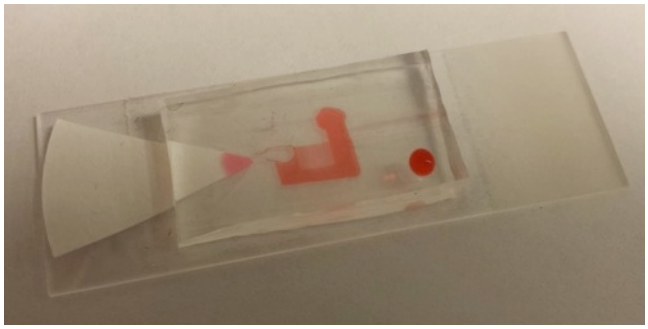

Figure 48 Example of a working self-pumping device

4.4.2 Self-Powered Pump Challenges

4.4.2.1 Bonding Issues

During the experiment, there were some issues with bonding with both the tape and plasma methods. There were several problems that came up when using the plasma bonding method however, so the tape method was primarily used.

With the tape method, there were inconsistencies in bonding strength; some trials had too strong of a bonding effect, while others were too weak. In the case of the strong bonding effects, liquid was less able to flow through the larger channels as they had been closed off. While the smaller channels were able to pass liquid, the design of the pump required a prefill to activate the pump. Initially the solution was to try different taping methods. Because of the particularly large design template, multiple pieces of tape were needed to ensure complete bonding. Numerous tape designs were attempted such as two single sided pieces, two double-sided pieces, one double sided piece, two double sided pieces with one single sided piece, etc., all of which yielded consistent results. The final solution to this problem was to precut the tape in order leave the large channels open. With this solution the larger channels were not bonded at all as the tape had been cut, allowing for fluid flow.

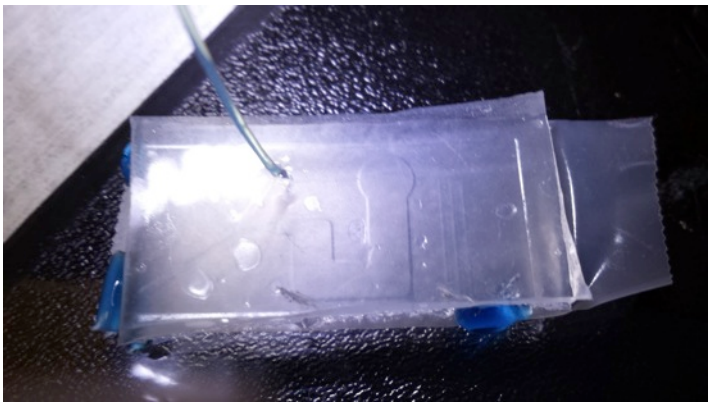

Figure 49 Larger channels are closed off and unable to allow flow

When the bonding effect was too weak, liquid would sometimes leak through the device. One potential solution was to create equal pressure prior bonding to ensure that the entire PDMS would stick to the tape. However this method proved to be difficult due to the sticky nature of PDMS. The PDMS was squeezed between two glass slides prior to baking, but when the second glass slide was pulled off the PDMS would stick to the second slide and would start peeling off the tape. An alternate method was to place a small weight on the device while it was baking. This method yielded more desirable results, but there were still some inconsistencies when it came to removing the weight. The removal of the weight would sometimes remain stuck to the PDMS and would peel it off the tape. Therefore, it was necessary to remove the weight carefully and slowly to ensure that the bonding remained intact.

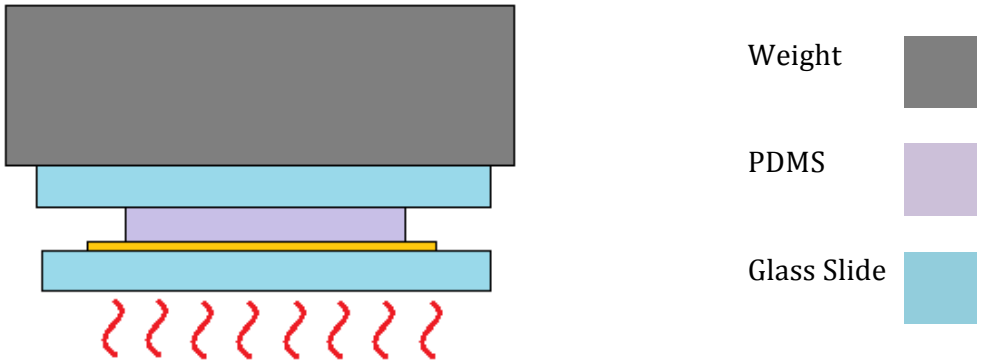

Figure 50 Example of set up with weight and legend

4.4.2.2 Leaking Issues

With the inconsistent bonding also came the leaking issues. In instances where the bonding was too weak, the liquid would flood the device and would also undo the bonding. The leaking was also related to the taping design for the bonding. As stated earlier, multiple tape designs were used; instances where two double-sided tapes were used, the leaking would occur where the two pieces were connected. A very small opening was created between the two pieces of tape. A third piece of one-sided tape was placed on top of the two pieces to attempt prevent the occurrence, however this proved to be ineffective. When these changes were implemented, flow insertion proceeded more smoothly as the devices were better suited for testing procedures.

Figure 51 Example of leaking device due to poor bonding

4.4.2.3 Air Bubbles

After prefilling the devices, the pump was activated so that the liquid could be absorbed by the filter paper to create flow. During this process, sometimes air bubbles would form in the larger channels, which prevented a smooth, continuous flow. It is unclear how they formed in the channels since the device was closed off from the air. This happened despite numerous attempts to create a vacuum free of air bubbles. These air bubbles however did not completely interfere with testing and results could still be obtained and the testing continued.

4.4.3 Suggestions

With future trials, it may be conducive to determine if different environment pressures would have any effect on the device on the device. This method may be possibly able to prevent the air bubbles from forming as well. To do this, the device would have to be fabricated in places where pressure can be controlled, such as a vacuum chamber or other special equipment. Testing would also need to be done in the pressure-controlled environments in order to determine how big of a factor pressure would be. Also, using less complicated larger channel shapes might be more effective for small dimensions. This or an entire template changes could be better for producing a constant flow

4.5 Modularity of the Device

One of the goals of this project is to have a modular system, that is, a device in which individual components can be added or replaced to improve its overall functionality. Particle separation by spiral channel was one such module that was investigated but was ultimately decided not to be used in the final device. The successful insertion and integration of optical fibers for flow detection as described in Section YY suggest that further modules that utilize the capabilities of optical fibers may be feasible.

4.5.1 Particle Separation by Spiral Channel Module

The team successfully fabricated spiral channel devices with various channel dimensions and radii of curvatures. , Blue and red polystyrene beads of with a diameter of 5 and 10 mm respectively were purchased from Phosphorex, Inc. 10 mliter of each sample were added to 5 mL solution of water. The final mixture was inserted into the spiral channel. The channel outlets were observed using a stereomicroscope with a video camera capable of delivering pictures at 30 frames per second. The bead samples were not visible when the flow speed was at 25ml/hr. When the pump was turned off and the flow started to move due to the pressure difference between the pressured syringe and the atmospheric pressure of the outlet, the large red beads where visible. However, no noticeable separation occurred. The blue bead samples where not visible under any flow speed. It is possible that an inverter microscope with high shutter speed video camera is more applicable of observing the separation of the samples. In addition, the spiral design required a high flow rate that could not be delivered using the self-power pump, nor sufficiently captured with a cellphone camera. For these reasons the team found that the spiral design would not desirable to be integrated with the final LoC device. However, this work can be further improved if optical tweezers are integrated. Optical tweezers is a method of utilizing light emitted from optical fibers to hold a particle in place. This technology could be used to hold the samples stationary while the images are being taken.

5. Discussion and Outlook

A project like this is not without challenges. Several challenges hindered progress and caused the direction of the project to shift. These challenges, as well as the overall results of this project and future applications of this technology are described in detail below.

5.1 Technical Challenges

Many technical challenges hindered the progress of this work. The plasma-bonding machine, used to initially bond devices to a glass substrate, did not function properly for a significant portion of the project when the team had access to it. The challenges presented by this machine prompted the study of the tape bonding technique, which presented its own challenges to the project. Certain types of tape proved to be more effective than others. The dimensions of the tape proved to be challenge: sometimes being too large to cut down properly for small devices or too small to bond smoothly for larger devices. By its very nature, tape is not a permanent bonding solution. As the background papers indicated [28], the team found that devices bonded to the tape would frequently become un-bonded during or after moderate testing.

Gluing the optical fibers in place also proved to be challenge. The amount of glue required to sufficiently hold a fiber in place would often make the chip uneven or unbalanced. Although the glue was expected to seal the channels guides for the optical fiber, the team encountered frequent leakage issues with this setup. More research on different types of glues could prove useful for future work.

Unfortunately, a fully functional optical fiber-based visual flow detection sensor was not fully implemented. Due to their small size, the tapered fibers being used for testing were easily broken or easily lost if they changed focal planes. Additionally, the fibers regularly got stuck to both the PDMS device and the adhesive tape substrate, and thus would not deform under a fluid flow. The speed of such a flow was also difficult to control, as leakage issues due to inefficient bonding altered the desired flow rate.

Some of the challenges encountered with imaging the microfluidic particles in the bead solution included determining optimal concentration and flow rate of the solution for imaging. The final concentration used was 3uL of 10% bead solution diluted in 3 mL of water, pumped at a flow speed of about 4 mm/s. Using the red beads in blue-dyed water enhanced the ability to image. However, keeping this solution stagnant for too long would render it unusable. As shown in Figure 52, the beads can get stuck to the plastic syringe if left unattended for extended periods of time.

Figure 52 Bead solution sitting stagnant for too long will cause the beads to sink and stick to the plastic syringe.

5.2 Simulation Challenges

One of the challenges the team faced was in obtaining accurate simulation. Finite element simulation could have been very useful in modeling the behavior of fluid flow through the microfluidic devices. However, due to time constraints and some unfamiliarity with the simulation tools, obtaining accurate simulation was forsaken in order to perform more testing.

The Dean flow in the spiral channel devices is a complex system for which computational analysis and optimization could have been useful. The CAD model of this system was imported from SolidWorks into COMSOL Multiphysics. Boundary conditions were set to 25 ml/h at the inlet, and zero pressure at the outlet. A water solution was chosen as the flowing medium. Figure 53 shows the result of the simulation.

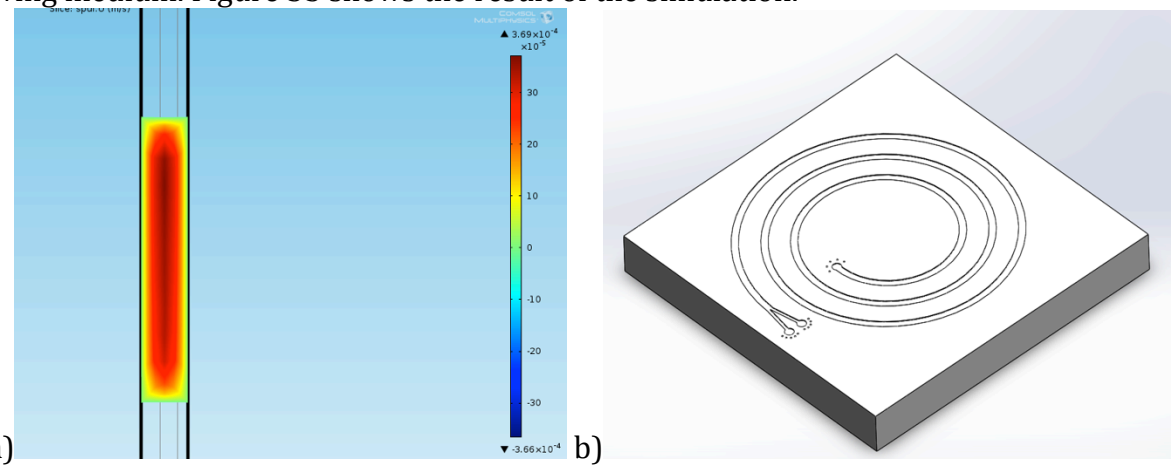

Figure 53 cross-sectional flow velocities in a spiral channel, moving upward b) Schematic view of the spiral device.

These results are not consistent with the expected Dean Flow phenomenon. Since the channel rotates upwards, the high flow speed should be in the bottom section of the channel instead of the top according to the principles of fluid inertia and the Dean flow. It was not determined why these simulation results were not consistent with expected behavior.

For the self-pump design, simulation was run to show how much the flow rate would increase as it reached the end of the fan area. Designs with fan angles of 20, 40, and 60 degrees were simulated, as shown in Figure 54 - Figure 56. The inlet channel for the large channel was selected as the fluid starting point, while the end of the fan area was selected as the endpoint.

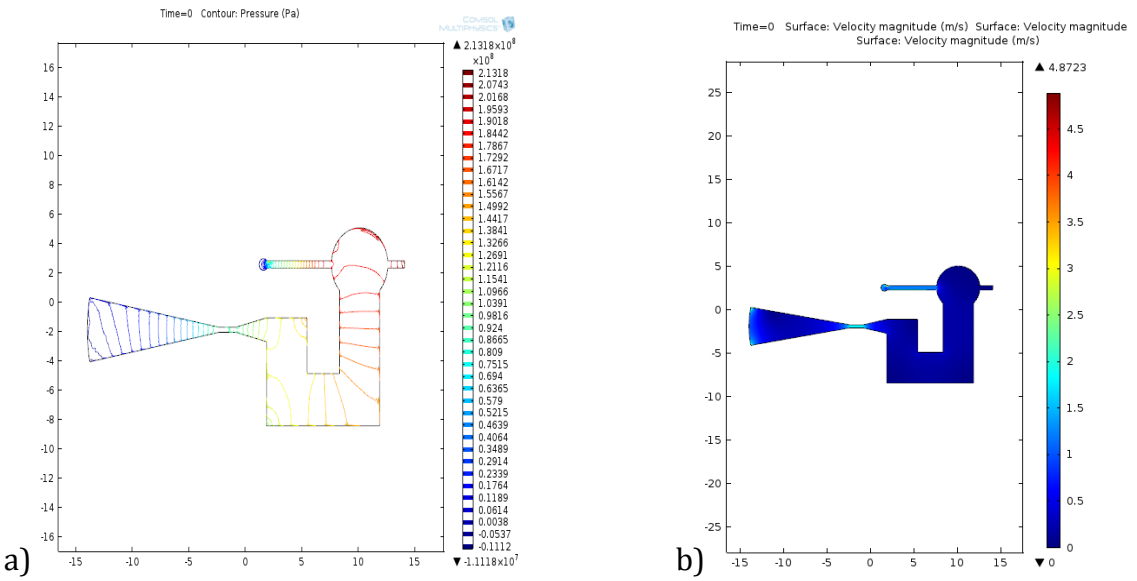

Figure 54 Simulation results of self-pump with fan at a 20-degree angle a) Pressure contour map b) Velocity magnitude

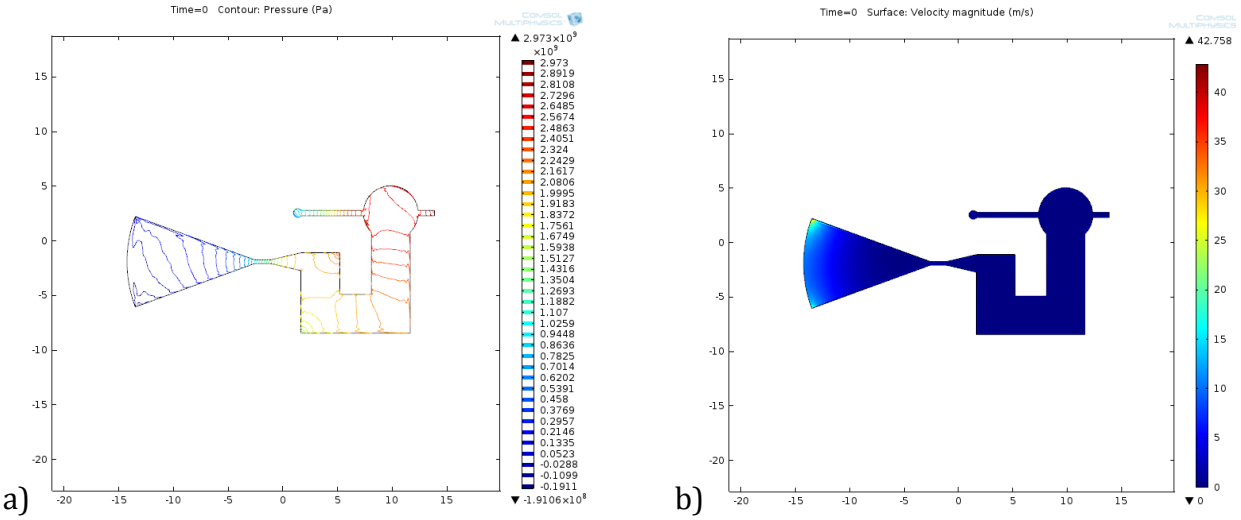

Figure 55 Simulation results of self-pump with fan at a 40-degree angle a) Pressure contour map b) Velocity magnitude

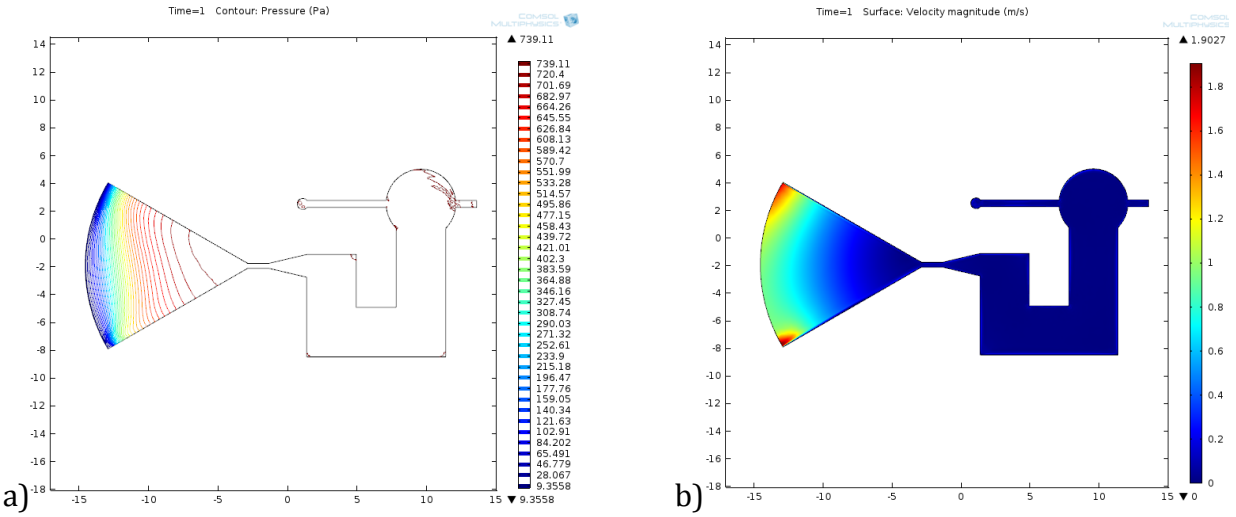

Figure 56 Simulation results of self-pump with fan at a 60-degree angle a) Pressure contour map b) Velocity magnitude

Because the device relies on the capillary effect to work, the device should start out with a high pressure, which should decrease near the end of the device. Overall, the simulation showed an almost constant pressure throughout the large channels while they slowly decrease in the fan area, as expected. However, the simulation for the fluid velocities was not consistent with the expected fluid behavior through different sized channels.

In the design, there is a very small channel that connects the large channels to the fan. In this area, the fluid velocity should have increased substantially, yet the simulation shows little to no change in the flow rate in the small channel. Another inconsistency is that the velocity should also increase near the end of the fan area. However, the simulation shows an increase on the very edge of the device. The fan should have a generally slow increase in the velocity as it reaches the edges.

One possible factor of these is the complexity of the channels. A more simple design may have more consistent results of the simulation. Additionally, because the features of the device are at such a small (micro) level, the program may not be able to process the small changes in in flow. When magnified though, there is the smallest of changes in velocity on the channel boundaries. The concern with this result however is that it should be bigger than what the simulation is showing. This could be due to incorrect boundary settings in the program. Another possibility could be the pressure. In this simulation, a constant low-pressure atmosphere was maintained. The changes may have been more visible if there was a change in pressure in the design. A low pressure in the beginning with a high pressure at the end would have been simulated. If that did not work, a constant high pressure would have been tested as well.

Ultimately, for the sake of time, simulation for the self-pump and spiral devices was not corrected to match the actual behavior of the fluids.

5.3 Personal Challenges

The leakage challenges resulting from the tape bonding illustrate one of several personal challenges encountered by the team. Due to unavailability of resources, including time, controlled testing with only one variable was not possible. New concepts such as the optical-fiber visual deformation for flow detection were tested with other new concepts, such as the tape bonding. As a result, the causes of unsuccessful tests were often difficult to identify. Because the goal of the project was to prove micro-mechanical concepts as opposed to performing sensitive biological experiments, standard sophisticated procedures for sanitary handling of the devices in sterile environments were not followed. This laxity likely affected the quality of the devices.

Due to the broad topic of the original MQP concept, the team found many different directions in which they were each passionate. The goal of having an integrated device with several novel components was too ambitious for the scope of the project. The successes of the project primarily occurred when the team members worked effectively together in close communication. The broad nature of this research-based MQP, unlike other projects in mechanical engineering, did not have a final product solution from the start of the project. Rather, recent relevant publications had the ability to abruptly change the direction of the project.

Another common issue was the time involved in working with third parties, including graduate students and outside vendors. This led to time being wasted because tests could not be conducted without certain materials or samples being fabricated. Less time could have been wasted with better planning and advanced ordering of products. Alternative procedures and tests could have been performed during such lulls.

5.4 Outlook

Future work could investigate alternative modules that could be integrated into one of these devices, or expand upon the modules described in this project. Further testing and implementation could be performed on the spiral channel-based separation modules and the fiber optical flow sensor. Additionally, working modules can be integrated into a single, fully functional and integrated device. Further application of fiber optics could also be added to increase functionality to the device. Fiber optics is a growing field of study that can be used for a variety of sensors beyond mere deformation-based flow sensing. Methods such as optical tweezing could be used to analyze and manipulate particles within the device.

Further integration of such fiber optical sensors with the smartphone is also possible. This project demonstrated a basic use of smartphone technology in Lab-on-a-Chip. If more advanced fiber sensors were used for data collection, that data could be computed and analyzed on a smartphone along with the visual analysis being performed. Such integration would greatly increase the functionality of the device and make the great potential of Lab-on-a-Chip technology more accessible to users outside of a laboratory setting.

6. Conclusion

This MQP developed a stand-alone, monolithic lab-on-a-chip device, with three integrated modules: self-powered pump, cellphone-based imaging platform, and on-chip fiber optical sensor. All the three modules are designed, fabricated, and tested. These functional components serve as building blocks that can be combined or replaced in a final design. By combining these individual, novel, microfluidic modules, this project conceptualized an integrated device removing the needs of a microscope or an external power supply for the pump. To the best of our knowledge, this is the first time all necessary functions of lab-on-a-chip devices, including pumping, characterization, and detection, are integrated on a single chip in which the only needed external device is a smartphone to work properly. Moreover, various techniques in the fabrication process were further developed such that the timespan of device fabrication were reduced by around 10 times. Prototype devices could be fabricated in a matter of hours instead of days. The MQP work can find applications in portable and disposable healthcare devices such as single-cell disease diagnosis and surface coating characterization.

References

1. E. K. Sackmann, A. L. Fulton, and D. J. Beebe, "The present and future role of microfluidics in biomedical research," Nature **507**, 181-189 (2014).

2. Y. H. Ghallab, and W. Badawy, "Lab-on-a-Chip: Techniques, Circuits, and Biomedical Applications," (Artech House, Norwood, MA, USA, 2010), p. 238.

3. "Amplitude Systemes, Lab-on-a-chip," http://www.amplitude-systemes.com/lab-on-chip.html2014.

4. Fair, R. B. (2007). Digital microfluidics: is a true lab-on-a-chip possible? *Microfluidics and Nanofluidics*, *3*(3), 245-281

5. M. W. Royal, N. M. Jokerst and R. B. Fair **"**Droplet-Based Sensing: Optical Microresonator Sensors Embedded in Digital Electrowetting Microfluidics Systems**"** *IEEE Sensors Journal,* vol. 13, no. 12, December 2013, pp. 4733-4742

6. Kokalj, T., Park, Y., Vencelj, M., Jenko, M., & Lee, L. P. (2014). Self-powered Imbibing Microfluidic Pump by Liquid Encapsulation: SIMPLE. Lab on a Chip.

7. Seo, Jeonggi, Meng H. Lean, and Ashutosh Kole. "Membrane-Free Microfiltration by Asymmetric Inertial Migration." Applied Physics Letters 75.3 (2007): 033901,033901-3. Print.

8. Sun, Jiashu, et al. "Double Spiral Microchannel for Label-Free Tumor Cell Separation and Enrichment." Lab on a chip 12.20 (2012): 3952. Print.

9. Martel, Joseph M., and Mehmet Toner. "Inertial Focusing in Microfluidics." *Annual review of biomedical engineering* 16 (2014): 371. Print.

10. Di Carlo, Dino. "Inertial Microfluidics." *Lab on a chip* 9.21 (2009): 3038. Print.

11. Amini, Hamed, Wonhee Lee, and Dino Di Carlo. "Inertial Microfluidic Physics." *Lab on a chip* 14.15 (2014): 2739. Print.

12. Densmore, A. Cheben, P.Xu, D. Janz, S.Waldron, P. Lapointe, J Schmid, J. H. (2008). Sensitive label-free biomolecular detection using thin silicon waveguides. Advances in Optical Technologies, 2008, 1-9. doi:10.1155/2008/725967

13. Quimby, Richard S. Photonics and Lasers: An Introduction. Hoboken, NJ: Wiley-Interscience, 2006. Print.

14. Lien, Victor, and Frank Vollmer. “Microfluidic flow rate detection based on integrated optical fiber cantilever” *Lab On A Chip*, 7 (2007); 1352. Print.

15. X. Heng, D. Erickson, R. Baugh, P. W. Sternberg, D. Psaltis, and C. Yang, "Optofluidic microscopy - a method for implementing a high resolution optical microscope on a chip," Lab On A Chip **6**, 1274 - 1276 (2006).

16. S. O. Isikman, W. Bishara, S. Mavandadim, F. W. Yu, S. Feng, R. Lau, and A. Ozcan, "Lens-free optical tomographic microscope with a large imaging volume on a chip," Proceeding of the National Academy of Sciences of the United States **108**, 7296 - 7301 (2011).

17. J. Wu, and M. Gu, "Microfluidic sensing: state of the art fabrication and detection techniques," Journal of Biomedical Optics **16** (2011).

18. J. Hecht, *Understanding Fiber Optics* (Pearson Prentice Hall, Upper Saddle River, New Jersey, 2006).

19. C. Jensen-McMullin, H. P. Lee, and E. R. Lyons, "Demonstration of trapping, motion control, sensing and fluorescence detection of polystyrene beads in a multi-fiber optical trap," Optics Express **13**, 2634-2642 (2005).

20. B. A. Flusberg, E. D. Cocker, W. Piyawattanametha, J. C. Jung, E. L. M. Cheung, and M. J. Schnitzer, "Fiber optic fluorescence imaging," **2**, 941-950 (2005).

21. C. C. Stemple, S. V. Angus, T. S. Park, and J.-Y. Yoon, "Smartphone-Based Optofluidic Lab-on-a-Chip for Detecting Pathogens from Blood," Journal of Laboratory Automation **19**, 35-41 (2014).

22. "Cell Phones Become Microscopes with 3-D Printing," (Phontonics.com, 2014).

23. "Mobile science," Nat Photon **8**, 745 (2014).

24. "PNNL Smartphone Microscope," (Pacific Northwest National Laboratory, 2014)2014. http://availabletechnologies.pnnl.gov/technology.asp?id=393

25. Source: C. A. Mack, "Semiconductor Lithography (Photolithography) - The Basic Process," (2014)

26. S. Bhattacharya, A. Datta, J. M. Berg, and S. Gangopadhyay, "Studies on Surface Wettability of Poly(Dimethyl) Siloxane (PDMS) and Glass Under Oxygen-Plasma Treatment and Correlation With Bond Strength," Journal of Microelectromechanical Systems **14**, 590 - 597 (2006).

27. E. Araci, "Designing Your Own Device: Chip Bonding," (Stanford Microfluidics Foundry).

28. Thompson, C. S., & Abate, A. R. (2013). Adhesive-based bonding technique for PDMS microfluidic devices. *Lab on a Chip*, *13*(4), 632-635.

29. "Making Flexible Molds with PDMS," (The Center of Excellence in Nanoelectronics, Indian Institute of Science, Bangalore, India, 2011).